Science of Remote Sensing 12 (2025) 100318

Contents lists available at ScienceDirect

Science of Remote Sensing

journal homepage: www.sciencedirect.com/journal/science-of-remote-sensing

Bridging spatio-temporal gaps in ALS data using Landsat time series and forest disturbance-recovery metrics via multi-task neural networks

Saverio Francini [a,*], Costanza Borghi [b], Giovanni D'Amico [b], Lars T. Waser [c], Maciej Lisiewicz [d], Krzysztof Stereńczak [d], Mart-Jan Schelhaas [e], Cameron Pellett [f], Terje Gobakken [g], Erik Næsset [g], Federico Magnani [a], Sergio de-Miguel [h], Gert-Jan Nabuurs [e], Ruben Valbuena [f], Gherardo Chirici [b]

[a] Department of Science and Technology of Agriculture and Environment (DISTAL), University of Bologna, 40126, Bologna, Italy
[b] Department of Agriculture, Food, Environment and Forest Science & Technology of University of Florence, Italy
[c] Land Change Science, Swiss Federal Institute for Forest, Snow and Landscape Research WSL, Switzerland
[d] Forest Research Institute, Department of Geomatics, Poland
[e] Wageningen University & Research, the Netherlands
[f] Swedish University of Agricultural Sciences, Sweden
[g] Faculty of Environmental Sciences and Natural Resource Management, Norwegian University of Life Sciences, Norway
[h] Department of Agricultural and Forest Sciences and Engineering, University of Lleida, Spain

A B S T R A C T

European forests contribute to climate change mitigation by sequestering carbon, conserving biodiversity, and enhancing water retention. However, climate-induced disturbances such as fires, windthrows, droughts, and pest outbreaks underscore the need for stronger forest monitoring systems. National Forest Inventories (NFIs) serve as the primary source of forest data and information in Europe. Yet, inconsistencies in timing, coverage, methodologies, and data quality highlight the need for a more harmonized and spatially detailed approach. Critically, predicting forest variables directly from satellite data remains challenging, mainly due to the difficulties in aligning remote sensing with ground data. Meanwhile, the operational use of airborne laser scanning (ALS) data is limited by high costs, infrequent updates, and inconsistent coverage from different sensors and flight conditions. This study presents a novel approach relying on fully connected neural networks to integrate Landsat satellite time series and forest disturbance and recovery metrics with ALS data to predict forest height metrics, which can then be used to accurately predict critical forest variables, such as growing stock volume (GSV) and stand basal area (BA). The method was tested across five ecologically and geographically diverse European forest regions: Tuscany (Italy), the Netherlands, the Canton of Grisons (Switzerland), Białowieża Forest (Poland), and the Vindelälven-Juhttátahkka Biosphere Reserve (Sweden). ALS forest height metrics were predicted with R^2 values ranging from 0.47 to 0.68. Then, based on field data, forest height metrics were used to predict GSV ($R^2 = 0.78$) and BA ($R^2 = 0.69$). Our method addresses the issue of limited spatial and temporal availability of ALS data by predicting ALS-derived height metrics using Landsat time series. This study examines the challenges of combining satellite and NFI data, building on the premise that satellite data can be effectively used to predict forest height metrics derived from ALS, which in turn can be used to accurately quantify several forest variables. The methods presented here support scalable and cost-effective forest monitoring by providing the spatially and temporally detailed information needed to implement climate-smart forestry.

1. Introduction

Forests cover more than one-third of the European land area (FISE, 2021) and provide a wide range of beneficial effects to the environment and citizens (Orsi et al., 2020), such as climate change mitigation (Petersson et al., 2022), carbon storage (Fahey et al., 2010), biodiversity conservation (Burrascano et al., 2023), and water retention (Ellison et al., 2017). Nevertheless, in the past decades, European forests experienced an increase in natural disturbances, possibly related to global warming (Palahí et al., 2021) and future scenarios forecast a serious increase in windthrow, fires, and insect attacks (Forzieri et al., 2021). Applying international policies to monitor, manage, and protect European forests against climate change and related threats is more pivotal than ever.

In this context, harmonized forest information is needed for international conventions involving forests, such as the United Nations Framework Convention on Climate Change and the Convention on Biological Diversity at the pan-European level. A large part of the

* Corresponding author.
E-mail address: saverio.francini@unibo.it (S. Francini).

https://doi.org/10.1016/j.srs.2025.100318
Received 4 June 2025; Received in revised form 7 July 2025; Accepted 22 October 2025
Available online 23 October 2025

required information is also crucial for supporting existing environmental policies in the EU, including the Sixth Environment Action Programme (Withana et al., 2010), the EU Biodiversity Strategy (Hermoso et al., 2022), the Habitats (European Commission, 1992), and Birds (European Commission, 1979) directives, the Thematic Strategy for Air Pollution (Skinner, 2006), the Nitrates Directive (Brouwer and Hellegers, 1996), the Water Framework Directive (European Commission, 2009), the Forest Action Plan, the EU Timber Regulation (Saunders and Reeve, 2014), and the Renewable Energy Directive (Schöpe, 2008). In 2023 such a need resulted in the proposal for a new regulation from the Directorate-General for the Environment of the European Commission "On a monitoring framework for resilient European forests" (COM (2023)728, November 22, 2023) aimed at setting up a comprehensive and high-quality forest monitoring system that covers all forests and other wooded land in the EU based on remotely sensed and ground data.

Currently, the ground component of forest monitoring is provided by the National Forest Inventories (NFIs), which serve as the primary data source for official statistics on European forests. Despite their valuable contributions, NFIs have relatively high costs, standardization issues, infrequent updates, and data access restrictions (Gessler et al., 2024). An effective European forest monitoring system should provide regularly updated, harmonized, reliable, wall-to-wall, and easy-to-use information on the state of forest ecosystems and the products and services they deliver, as well as monitor biodiversity and sustainable forest management practices within emerging bioeconomy markets. NFIs alone do not satisfy all these requirements.

In recent years, the availability of remotely sensed data has increased substantially (Wulder and Coops, 2014). Along with advances in cloud computing (Gomes et al., 2020; Gorelick et al., 2017), this has enabled the application of more sophisticated algorithms over larger areas (Francini et al., 2022b), critical to retrieve information on forest structures and dynamics (Matasci et al., 2018b). However, while a huge amount of satellite data is freely available for the whole globe and with high spatial and temporal resolutions, predicting forest variables directly from optical data is challenging and often results in low accuracy, mainly due to i) the signal saturation effects because of the optical sensors' limited capability to retrieve information in densely vegetated areas (Avitabile et al., 2012; Healey et al., 2020) and ii) the incapability of medium resolution optical data in measuring the 3D structure of the forest and the related features (Su et al., 2016). In addition, the spatial resolution of satellite data is usually too coarse to properly compare pixels and ground data obtained from NFIs, since a pixel can only partially overlap with the ground plot (Francini et al., 2024). This last issue is amplified by the imprecision of ground plot coordinates and by model predictions based on remotely sensed data, which can be inaccurate for individual pixels (Chirici et al., 2020; McRoberts and Tomppo, 2007).

On the other hand, airborne laser scanner (ALS) technological advancements have revolutionized forest structure data capture, transitioning from experimental to operational use due to decreasing costs and increased availability of sensors (Nelson, 2013). Overall, ALS complements field measurements and optical data by providing three-dimensional (3D) forest structure information (Puliti et al., 2018; Ståhl et al., 2016). Indeed, ALS data have been proven highly effective for estimating growing stock volume (GSV) (Næsset, E. 1997, Næsset, E. 2002; Bolton et al., 2020; Breidenbach et al., 2010; Cartus et al., 2012), aboveground biomass (Almeida et al., 2021; Margolis et al., 2015; Mascaro et al., 2011; Næsset and Gobakken, 2008), measuring height metrics (Næsset, 1997b, 2002; Villikka et al., 2012; Alvites et al., 2025), habitat (Müller and Brandl, 2009), tree species (Gong et al., 2024; Ørka et al., 2009, 2010; Shi et al., 2018) and tree species diversity (Almeida et al., 2021; Erfanifard et al., 2024; Davies and Asner, 2014), and quantifying forest ecosystem services (Vauhkonen, 2018; Van Stan et al., 2017). Despite their huge potential and the key role they could play in European forest monitoring, ALS data are available only for limited study areas and do not cover all EU forests. ALS acquisitions remain expensive compared to other data sources and are thus updated rarely. Finally, ALS data are acquired by different sensors and collected during flights performed at various altitudes and in different years. As a result, only a portion of European forests are covered by ALS data, with acquisitions spread randomly over several years and with different point densities complicating the task of harmonization and resulting in critical information gaps. In summary, each data stream (satellite, ALS, and NFI) presents limitations in monitoring European forests when used alone, but larger potential lies in their combination (Matasci et al., 2018).

Specifically, predicting ALS forest structure data from optical satellite data would enable data provision in European areas where ALS data is currently unavailable, and would facilitate more frequent updates of ALS data. Specifically, having access to comprehensive, wall-to-wall, and annual or sub-annual updated ALS data would facilitate the quantification of numerous indicators essential for supporting the implementation of optimized management practices and policies for European forests in a climate change scenario. Indeed, the integration of satellite, ALS, and field inventory data is becoming a key component of modern forest monitoring (de Lera Garrido et al., 2023; Liu et al., 2023; Fassnacht et al., 2024). This multi-source approach combines the broad coverage of satellites, the structural detail of ALS, and the accuracy of field data to estimate forest attributes such as volume, basal area, and canopy height (Matasci et al., 2018a). Some of the methods relying on such multi-source data are known as hierarchical modeling frameworks. These use ALS data as an intermediate layer between satellite and field data (Lang et al., 2022; Schwartz et al., 2023), which has proven effective in improving prediction accuracy and in overcoming issues associated with satellite-ground data direct combination (Pflugmacher et al., 2014; Miettinen et al., 2025). Indeed, ALS data cover larger areas than ground plots and enable the calculation of height metrics in remote or inaccessible areas and at a more compatible spatial resolution than ground data, which facilitates integration with satellite data (Zald et al., 2016; Wulder and Coops, 2014; Wulder et al., 2012a; Matasci et al., 2018b).

Critically, recent advancements in deep learning and data fusion further enhance the predictive power of satellite-ALS-ground data hierarchical methods (Tolan et al., 2024; Fogel et al., 2024), with fully connected neural networks (FCNNs) often being a first choice for modeling forest characteristics such as GSV (Hawryło et al., 2020), or supporting forest management and planning through the automatic classification of high-resolution satellite imagery (D'Amico et al., 2021a). In particular, FCNNs have proven particularly effective for simultaneously predicting multiple correlated continuous variables due to their ability to capture complex relationships and share informative representations across tasks (Caruana, 1997; Zhang et al., 2019). On the other hand, such models have not been applied so far to predict forest height metrics measured by ALS from Landsat data. Also, while Landsat time series enables us to accurately retrieve critical information on forest disturbances (Kennedy et al., 2010; Hansen et al., 2013; Hermosilla et al., 2015) and recovery (White et al., 2016; 2018), and while such information are expected to be a critical junction point between optical satellite and forest structure variables (Matasci et al., 2018), such path is underexplored, with any relevant application in the EU context.

By leveraging recent advances in FCNN-based multivariate modeling (Tolan et al., 2024), state-of-the-art pixel compositing techniques (Francini et al., 2024), and long-term Landsat-based disturbance (Hermosilla et al., 2015) and recovery metrics (White et al., 2016), this study proposes a novel two-step approach to integrate satellite and ALS data for forest monitoring. Specifically, we demonstrate across five ecologically and geographically very diverse European regions that sparse and heterogeneous ALS and ground datasets can be effectively combined with dense satellite time series to predict forest height metrics. These predicted height metrics are then used to estimate GSV and basal area (BA) through a second FCNN. This hierarchical framework not only addresses the lack of consistent ALS coverage but also provides a scalable pathway for harmonized forest structural mapping across

national and regional boundaries.

2. Test areas

The study was carried out in five areas of Europe representing very different ecosystems and climate conditions, and for which we collected and processed NFI or ground data, ALS data, and satellite data: (i) the Vindelälven-Juhttátahkka Biosphere Reserve (Sweden), (ii) the entire country of The Netherlands, (iii) the Białowieża forest (Poland), (iv) the Canton of Grisons (Switzerland), and (v) the Tuscany Italian administrative region (Fig. 1).

The Vindelälven-Juhttátahkka Biosphere Reserve is located in northern Sweden and spans an area of approximately 13,000 km^2, with a forest area of around 7900 km^2, accounting for 53 % of the entire reserve. The reserve spans alpine, inland, and coastal regions, with forests dominated by Scots pine and Norway spruce. In the Netherlands, the forested area is approximately 3700 km^2, accounting for 11 % of the total land area, and features a relatively diverse species distribution resulting from differences in forest history, site conditions, and changes in species preferences over time. The Białowieża Forest is situated between Poland and Belarus; however, this study focuses on the 592 km^2 area that belongs solely to Poland. The Canton of Grisons in Switzerland is characterized by an elevation range of 253–4048 m and by large geographical and topographical variability. It covers 7105 km^2 of the Aplin arc and contains 2100 km^2 of forests. Lastly, Tuscany (23,000 km^2) is situated in central Italy and encompasses approximately 11,000 km^2 of forests over a territory that ranges from the sea to mountains of 2000 m.

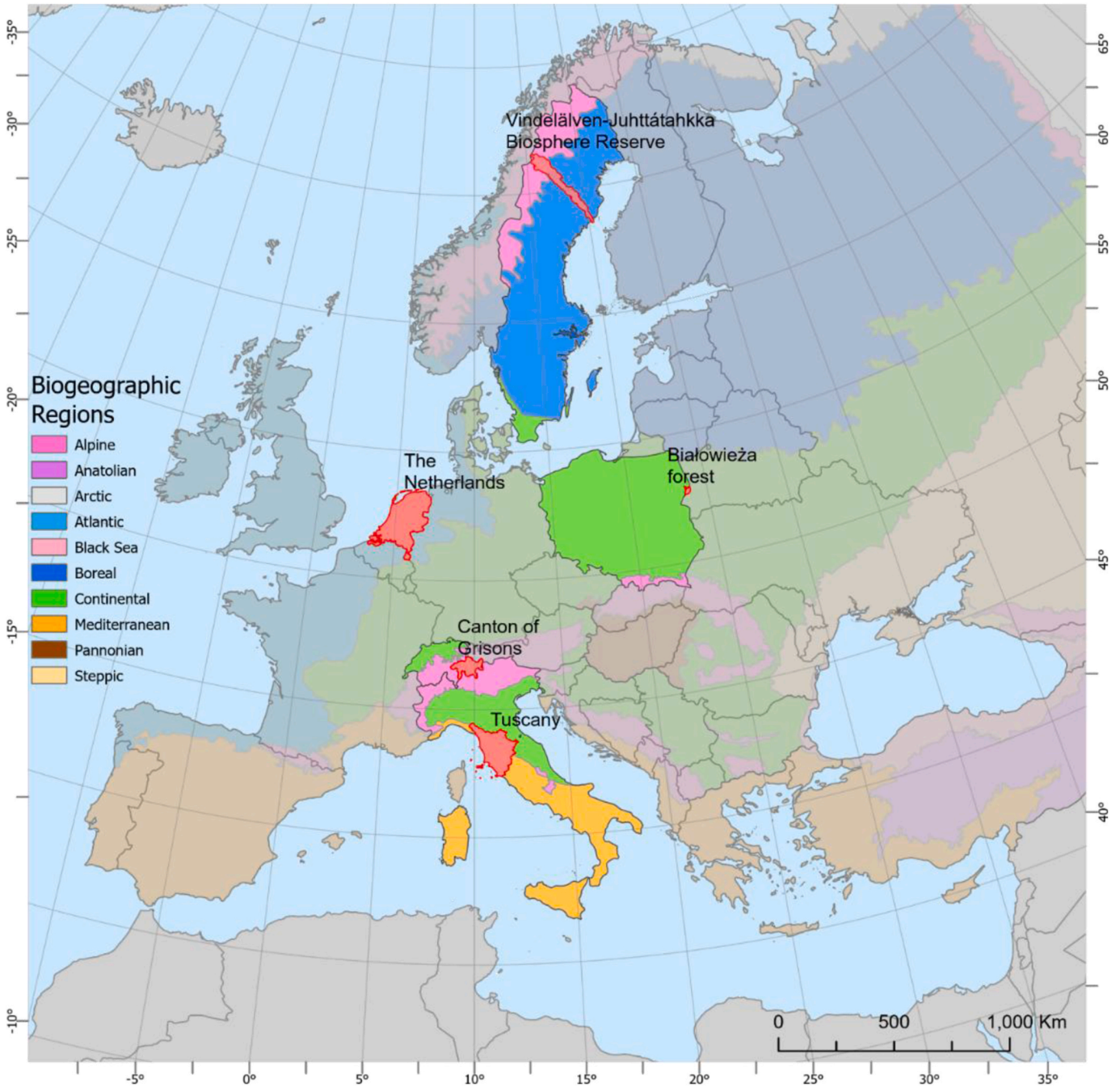

Fig. 1. – *Spatial distribution across biogeographic regions (EEA, 2016) of the study areas: (i) Vindelälven-Juhttátahkka Biosphere Reserve (Sweden), (ii) The Netherlands, (iii) the Białowieża Forest (Poland), (iv) Canton of Grisons (Switzerland), (v) Tuscany (Italy).*

To properly test the applicability of our method at the European level, these study areas encompass diverse biogeographic regions, varying climate conditions (Fig. 1), a range of forest species, and different forest management regimes (Table 1).

3. Data

3.1. Determination of forest areas

To map forested areas, we utilized local forest maps validated by local authorities. These forest maps were created using various methods, but are all grounded in the FAO definition, which is employed to generate official forest area statistics in Europe based on NFIs (McRoberts et al., 2009). According to the FAO definition, temporary unstocked forests are classified as forests in these masks. To match the spatial resolution of the Landsat imagery used in this study, all forest masks were resampled to a spatial resolution of 30 m and harmonized into binary forest/no-forest masks. For more information on these masks and relevant references, see the forest mask column in Table 1.

3.2. Landsat data

In this study, we used Landsat imagery, which provides comprehensive coverage of the Earth's surface at a 30-m resolution of multispectral optical data. Although the more recent Copernicus Sentinel constellation is providing novel data, and while this data will play a crucial role in forest monitoring, the Landsat consistent, continuous, and long (since 1984) acquisitions make it one of the most valuable sources of information for long-term forest disturbance monitoring (Coppin and Bauer, 1996; Wulder et al., 2022) and forest disturbance detection (Borghi et al., 2021; Hansen et al., 2013; Hermosilla et al., 2015; Kennedy et al., 2010). Landsat provides near-nadir observations at medium spatial (30 m) and temporal (8–18 days) resolutions.

In this study, we used Landsat imagery acquired between 1984 and 2022, belonging to the most updated dataset (Landsat Collection 2) as provided by Google Earth Engine (GEE), a cloud-based platform with high-performance and planetary-scale computing resources for processing vast geospatial datasets (Gorelick et al., 2017).

3.3. Airborne laser scanning data

For each study area, we collected available canopy height models (CHMs) at different spatial resolutions. All of them were produced due to the difference between the digital surface model and the digital terrain model. As a result of discrepancies in flight altitudes and acquisition years across the five study areas, point densities of ALS data used to construct the CHMs were different (Table 2). These very different CHMs simulate the real availability of ALS data in Europe and, in this study, were harmonized at a later stage by constructing ALS plots (see section 4.4).

Table 1
Summary information on test areas.

Study area	Forest mask	Forest area	Main tree species
(i) Vindelälven-Juhttátahkka Biosphere Reserve, SE	10 m, 2017–2019, (Nilsson et al., 2017).	7896 km^2	*Picea abies, Pinus sylvestris, Betula pendula*
(ii) The Netherlands	25 m, 2017Arets et al. (2019)	3700 km^2	*Pinus sylvestris, Quercus* sp.
(iii) Białowieża forest, PL	Vector (Forest Data Bank, 2024)	592 km^2	*Alnus glutinosa, Carpinus betulus, Picea abies, Pinus sylvestris, Betula* spp., *Quercus* spp.
(iv) Canton of Grisons, CH	10 m, 2021 (Ginzler and Hobi, 2015)	2100 km^2	*Picea abies, Pinus sylvestris, Larix decidua, Fagus sylvatica, Fraxinus excelsior,*
(v) Tuscany, IT	23 m, 2012–2018 (D'Amico et al., 2021b)	11,000 km^2	*Quercus* spp., *Pinus pinaster, Pinus nigra*

3.4. Ground data

Ground data used in the study were mostly derived from NFIs, which differed in plot dimensions and measured metrics (Table 3). Further, we identified relevant differences in the minimum diameter for measurement, the minimum branch diameter for inclusion in GSV calculation, and in the number of measured heights per plot, for which we provide detailed information in Annex D.

4. Methodology

We characterized the forest's historical (1985–2022) spectral behavior, mapped forest disturbances, predicted forest 3D structure, and, finally, predicted key forest variables. The methodology is articulated in several steps (Fig. 2), and each step requires different input parameters that were calibrated for each of the five study areas (Table C.1 in annex C).

4.1. Best available pixel mosaicking and spectral indices

To produce yearly cloud-free mosaics of Landsat scenes, we used the best available pixel (BAP) compositing algorithm. The key elements of the BAP methodology are summarized below, while a more detailed description of the approach and the criteria it relies on can be found in Griffiths et al. (2013) and White et al. (2014).

Using the BAP, the "best" pixels from those available in a pre-defined time window are selected based on four scoring functions which rank observations based on: i) acquisition sensor, ii) proximity of acquisition date to the target date (based on the day of the year -DOY), iii) distance to the cloud or cloud shadows (Griffiths et al., 2013; Foga et al., 2017), and iv) atmospheric opacity (Schmidt et al., 2013). The sensor scoring function serves to mitigate the impact of spatial gaps associated with Landsat-7 ETM + scan line corrector-off data. Thus, a lower sensor score is assigned to all pixels acquired by Landsat 7 after 2003-May-31, while all Landsat 8 pixels and Landsat 7 pixels acquired before 2003-May-31 receive the full sensor score.

In this study, the target date coincided with the central date of the periods used for constructing the composites in each study area (White et al., 2014). Due to seasonality, consequent cloud coverage, and imagery availability, the periods and the target date used to construct the composites change depending on the study area (Table C.1). According to the BAP algorithm, pixels of images acquired closer to the target date are scored higher and are therefore preferentially selected.

Table 2
Summary information on ALS data used in this study.

Study area	Area (km^2)	Density (pts m^{-2})	Flight altitude (m)	year	CHM resolution (m)
(i) Vindelälven-Juhttátahkka Biosphere Reserve, SE	14870	1–2	3000	2018	2
(ii) Białowieża Forest, PL	590	19	844–890	2019	1
(iii) The Netherlands	560	16	~1000, but varies due to local restrictions)	2017	0.5
(iv) Canton of Grisons, CH	720	15–20	1500–3200	2021	0.5
(v) Tuscany, IT	4740	1.6	1050–1300	2008	1

Table 3
Summary information on ground data.

Study area	N° plots	Year	Plot radius (m)	Average volume (m^3 ha^{-1})
(i) Vindelälven-Juhttátahkka Biosphere Reserve, SE	1072	2007–2021	7	102
(ii) Białowieża Forest, PL	672	2015 2017 2019	12.62	469
(iii) The Netherlands	1398	2013	5–20	224
(iv) Canton of Grisons, CH	900	2017	12.62	354
(v) Tuscany, IT	707	2005	13	136

Through the BAP algorithm, we obtained cloud-free mosaics for all Landsat bands for all the study areas and each year between 1984 and 2022. Such data were then used to produce images of the following spectral indices (Lillesand et al., 2015): (i) normalized difference vegetation index (NDVI), (ii) normalized burned ratio (NBR), (iii) Enhanced Vegetation Index (EVI), and (iv) Tasseled Cap Brightness, Wetness, Greenness, and Angle (TCB, TCW, TCG, TCA). The codes for implementing the BAP algorithm and calculating spectral indices are available on both GitHub (https://github.com/saveriofrancini/bap) and Google Earth Engine (https://code.earthengine.google.com/?accept_repo=users/sfrancini/bap), while a procedure to assess the BAP outputs is provided in Francini et al. (2023b).

4.2. Despiking algorithm

To reduce noisy or corrupted pixels coming from unscreened clouds, cloud shadows, haze, or smoke, we used a despiking algorithm (Kennedy et al., 2010), based on the analysis of each pixel time series, independently for each one of the six Landsat spectral bands (Hermosilla et al., 2015). Specifically, a pixel was flagged as noise if (i) the difference between the spectral value in the year under consideration (e.g., 2000) and the average of the previous and subsequent years (e.g., 1999 and 2001) exceeded a despiking threshold (Table C.1) in half or more of the Landsat bands considered AND (ii) the value of the spike detected in that band was greater than 100. Where the spike is the absolute difference between pixel values in the year of analysis and the average between previous and subsequent years. Finally, detected spikes were filled through linear interpolation of band values in the previous and subsequent years (Francini et al., 2023a).

The despiking algorithm was applied to all images between 1985 and 2021. Because the despiking algorithm required imagery of previous and subsequent years, it was not applied to the images belonging to the start (1984) and end (2022) years of the time series.

4.3. Temporal segmentation and change metrics calculation

While due to the saturation issue, optical data present some challenges in predicting 3D forest structure, optical data is known to be very effective in mapping forest disturbances, which, in turn, are expected to be very informative in predicting biomass and forest structure.

To calculate temporal change metrics from Landsat BAP composites, a time-series temporal segmentation process was used (Keogh et al., 2004). These algorithms increase the signal-to-noise ratio by removing redundant information while detecting meaningful segments and breakpoints in the time series. A breakpoint signifies a shift in the temporal evolution of a pixel's values over time. To detect these breakpoints, we analyzed the time series of the Normalized Burn Ratio (NBR; Key and Benson, 2006), a metric recognized for its sensitivity and reliability in identifying disturbance events in forest environments (Kennedy et al., 2010). Our temporal segmentation method is based on a refined version of the Sliding Window and Bottom-Up algorithm (Keogh et al., 2001). First, for each pixel time series, the finest possible approximation was created by merging all pairs of adjacent points. In this way, the time series is represented as a set of N-1 segments, where N is the number of valid observations for that pixel. Second, we calculate the *cost* of merging each pair of adjacent segments. Then, we remove the breakpoint between the two segments that can be merged with the lower *cost*. Where the *cost* is calculated as the average absolute difference (in terms of NBR) between the new eventual segment and all of the original existing vertices. The second step is then repeated until the number of segments OR the RMSE does not exceed their thresholds (maximum segments and maximum RMSE, respectively, Table C.1). Pre-change,

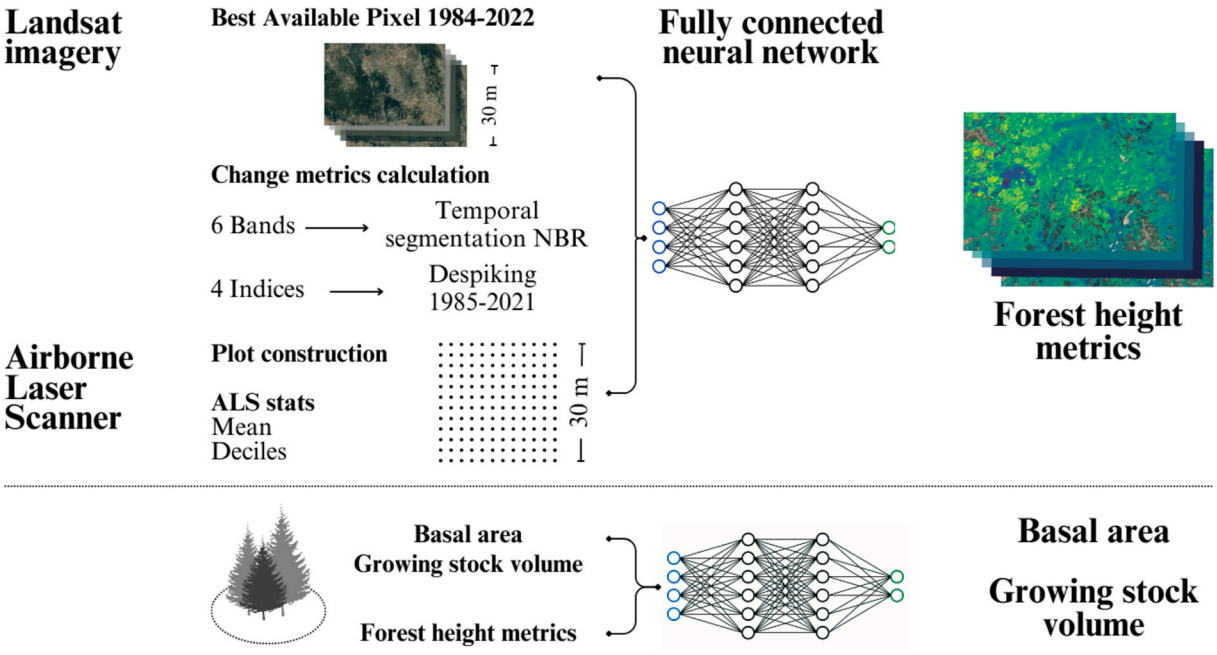

Fig. 2. Methodology workflow. Top, a schematic representation of the data used and steps implemented to obtain forest height metrics maps by combining satellite and ALS data. Bottom, the model was implemented to link forest height metrics with growing stock volume and basal area.

change, and post-change temporal metrics provide information on change year, magnitude, persistence, and rate.

. Several details on temporal feature calculation can be found in Hermosilla et al. (2015). A detailed description and references for the temporal change metrics used in the study can be found in Annex A.

For each pixel and year of analysis, for each one of the six bands (blue, green, red, NIR, SWIR, SWIR 2) and eight spectral indices considered (NDVI, NBR, EVI, TCB, TCG, TCW, TCA, DOY), we analyzed the temporal trajectories by calculating a set of three temporal change metrics. Pre- and post-variations were calculated to characterize the change events as well as pre-and post-change conditions to calculate the following temporal change metrics: the year in which the greatest disturbance of the time series occurred, the magnitude of that disturbance, and the total number of breakpoints detected in the time series by the temporal segmentation algorithm.

This metric was not considered in previous studies but can provide important insights as, depending on the year and imagery availability, a pixel can be acquired in slightly different periods (e.g., June or August), and thus different phenological conditions. For each year, also the numbers of years to previous and subsequent breakpoints were calculated, giving insights into (i) forest disturbance duration, and (ii) the rate of changes to subsequent years.

As a result of this step, we obtained a set of 33 change metrics which, along with the spectral bands (6), indices (7), and the additional DOY band calculated using BAP (see Section 4.1), form a total of 48 predictors to be related with ALS forest height (see Table 1 in Annex A for further details).

4.4. ALS plots construction

ALS plots are defined areas of a fixed radius or size for which ALS metrics and statistics are calculated. Critically, ALS plots can be established to acquire relevant forest information while reducing costs associated with ground reference data acquisition over large areas (Andersen, 2009). Within this study, we propose to use data from ALS as a surrogate for data obtained in plots during fieldwork and to provide a spatially extensive and detailed source of forest attribute information. We constructed ALS plots as squares with 30-m sides to match the size of Landsat pixels – our ALS reference dataset consists of all Landsat-sized pixels within the ALS-covered areas. The forest height metrics we calculated for each ALS plot are the tree height mean and deciles. More details on the procedure for constructing the ALS plots are provided by Matasci et al. (2018b).

4.5. Fully connected neural network: forest height metrics and forest structure prediction

Deep learning models were used in this study in two different steps: first, to predict tree height metrics from Landsat data, and second, to predict forest variables (e.g., GSV and BA) from forest height metrics measured on the ground.

Neural networks and deep learning models can return multiple response variables at once. Deep learning models consist of a series of stacked layers composed of nodes that facilitate learning through successive representations of the input data (Heaton, 2018). Here, we exploited fully connected neural networks (FCNN), i.e., neural networks in which all nodes or neurons in one layer are connected to the nodes in the next layer. The data are transformed in each layer using weights, which are specific parameters that link the nodes of subsequent layers (Hawryło et al., 2020). The FCNN hyperparameters setting was performed using a trial-and-error approach, which resulted in the configuration shown in Fig. 3.

Activation functions are used in neural networks to merge multiple inputs and to decide if a neuron can be fired or not (Nwankpa et al.,

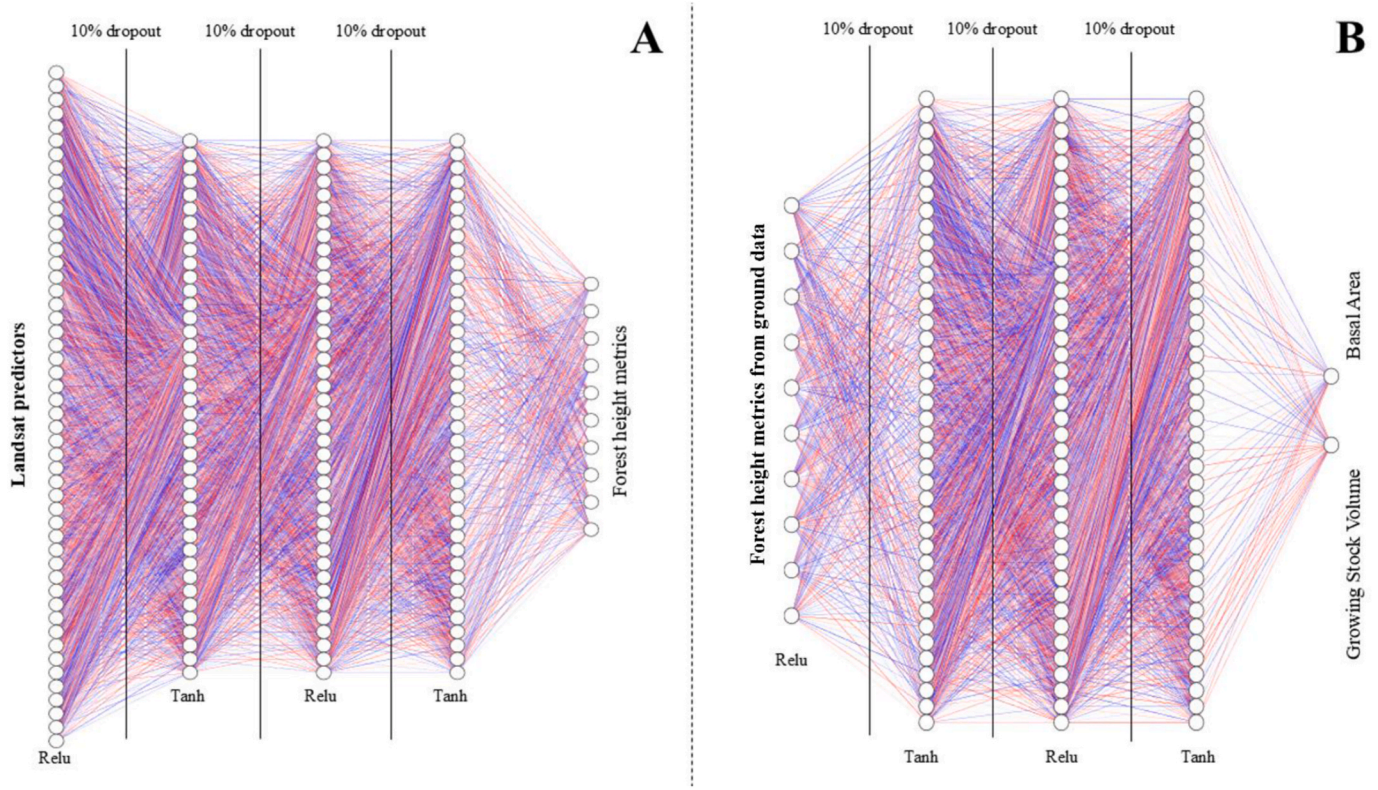

Fig. 3. Fully connected neural network (FCNN) configuration. The first neural network (panel A) is trained with ALS data to predict forest height metrics from Landsat predictors while the second one is trained with ground data (panel B) to predict growing stock volume and basal area from the predicted forest height metrics.

2018). The first activation function used in this study is the Rectified Linear Unit (ReLU) function (Eq. (1)), which sets to 0 negative values.

$$f(x) = max(0, x) = \{x_i, if\ x_i \geq 0\ 0, if\ x_i < 0 \quad (1)$$

ReLU returns 0 if the input (x) value is smaller than or equal to 0; otherwise, it returns x. Second, a hyperbolic tangent (Tanh) function (Eq. (2)) was used. Tanh is an S-shaped curve passing through the origin that, in this case, modifies the positive values produced by ReLU, returning a rapid increase for small values and an asymptotic flattening to 1 for large ones.

$$f(x) = \left(\frac{e^x - e^{-x}}{e^x + e^{-x}}\right) \quad (2)$$

To prevent overfitting and to ensure model generalizability, we used the dropout layer's function that serves to randomly discard some nodes (in our case 10 %) from the network during each training session. Because each training sub-network is different, it is possible to prevent the FCNN from overfitting the training data, to improve the generalization and its ability (Srivastava et al., 2014). The network was trained for 10k epochs using the mean square error loss function and the RMSprop optimizer, implemented in the TensorFlow (https://www.tensorflow.org/) and Keras (https://keras.io/) APIs.

Both neural networks (Fig. 3) were trained using 60 % of the data, while 20 % of the data was used to evaluate the loss function and decide when to stop training the network. The remaining 20 % served as never-seen-before data that was not in any way exploited by the model and that can be thus used to assess model performance. Accuracy was calculated for both models (that predicting forest height metrics and that predicting GSV and BA) in terms of Pearson correlation coefficient and root mean square error, calculated independently for each predicted variable.

More details on the procedure to implement, train, validate, and test the FCNN are provided by D'Amico et al. (2021a) while codes and main functions are provided along with the TensorFlow R package (https://tensorflow.rstudio.com/).

For each study area, the number of observations used in the first neural network – that for predicting forest height metrics – varied depending on the number of available ALS plots, while for the second network – that predicting GSV and BA based on forest height metrics measured in the ground – it varied based on the number of available plots.

5. Results

As a result of the BAP compositing algorithm application, we obtained time series (1984–2022) of pan-European pixel-based cloud-free Landsat composites (for each one of the six bands and eight spectral indices). Through the temporal segmentation process, BAP composites were used to calculate the temporal change metrics over the five study areas (Fig. 4).

Using the BAP yearly mosaics bands, spectral indices, and temporal change metrics (for a total of 46 Landsat-derived predictors, see Annex A), we accurately modeled ALS height metrics for the five study areas. Fig. 5 shows the comparison between the forest height metrics calculated from the ALS data available and the forest height metrics predicted using the FCNN in the Vindelälven-Juhttátahkka Biosphere Reserve (Sweden) while the results obtained for the other four study areas are available in Annex B. For each scatter plot, both the RMSE and the R^2 calculated over the test datasets are reported. For comparison purposes, the latter is shown for each study area and metric in Fig. 6. Results show R^2 ranging between 0.53 and 0.72 and RMSE values ranging between 2.2 and 5.7 m.

According to Fig. 6, the greatest accuracy was reached for the study area in Sweden, followed by Białowieża and the Netherlands, and finally, Tuscany and Switzerland. The average R^2 for Tuscany and Switzerland were 0.5 and 0.47, encouraging accuracies compared to similar studies (Hettema et al., 2022; Potapov et al., 2021).

To demonstrate the usefulness of the predicted forest height metrics, we combined forest height metrics measured on the ground with the respective GSV and BA at the plot level. Results for the Vindelälven-Juhttátahkka Biosphere Reserve are in Fig. 7, while results for all the other study areas are in Annex B, Figs. 1b–4b. Across the five areas, the average R^2 for GSV was 0.8, while for BA it was 0.78 (Fig. 8).

6. Discussion

This study demonstrates the potential of integrating Landsat imagery and derived forest disturbance and recovery metrics with ALS data and ground-based measurements into a scalable framework for forest monitoring, building on and integrating ideas and methods from previous knowledge (Matasci et al., 2018, White et al., 2014, D'Amico et al., 2022; Gregoire et al., 2016). The combination of these datasets addresses the limitations of traditional NFIs, which are often constrained by high costs, infrequent updates, and variability in standardization. By leveraging remote sensing data and advanced algorithms such FCNNs, this study offers an efficient method for generating wall-to-wall essential and comparable forest structure information, supporting sustainable forest management practices.

The integration of optical satellite data and ALS-derived metrics provides substantial advancements in forest monitoring. In this study, long-time series of Landsat data were used accurately to predict ALS-derived height metrics and, in turn, forest structural variables such as GSV and BA. Across the five study areas, height metrics were predicted with R^2 values ranging from 0.47 (Canton of Grisons) to 0.68 (Sweden), with such differences in accuracy mainly related to diverse data quality as discussed later in this section. This achievement highlights the potential to estimate forest characteristics even in remote or inaccessible regions, despite the availability of ALS data (Puliti et al., 2018; Saarela et al., 2016, 2018).

Importantly, in this study, we used fully connected neural networks (FCNN) to simultaneously predict multiple continuous variables that are strongly correlated, that is, the forest height percentiles or GSV and BA. This approach is grounded in the multi-task learning (MTL) paradigm, where a single model learns shared representations to improve generalization across tasks (Caruana, 1997). When output variables are correlated, FCNNs and MTL offer clear advantages over training independent models: they reduce the risk of overfitting, make more efficient use of the data, and exploit inter-variable dependencies to enhance overall predictive performance (Reichstein et al., 2019; Ayzel et al., 2019). Although more computationally demanding (Delgado-Fernández et al., 2014), FCNNs also scale better for multi-output regression compared to alternative models such as Random Forests (Breidenbach et al., 2010), due to parameter sharing and end-to-end optimization (Zhou et al., 2002; Zhang et al., 2019; Du et al., 2021; Fan et al., 2024; Omoniyi and Sims, 2024, Seely et al., 2025). The use of FCNNs in the joint modeling of multiple correlated variables has been shown to enhance prediction stability and generalizability (Schwartz et al., 2023; Liu et al., 2023; de Lera Garrido et al., 2023). Together, these studies reinforce the importance of integrating multi-source data within flexible, multivariate modeling frameworks like FCNNs. The accuracy we obtained is indeed promising compared to previous studies.

Hudak et al. (2002) used Landsat to predict forest height metrics, testing different models and with an R^2 up to 0.88 (using regression + cokriging), but using kriging alone, the R^2 was 0.29. Also, the study focused on a single and relatively small study area, which facilitates accurate model predictions. Staben et al. (2018) used Landsat 5, 7, and 8 data and RF to predict canopy height metrics with an R^2 of 0.49–0.53 over a study area of 1800 km^2. They also analyzed how the R^2 varies across different forest ecosystems and found a range between 0.32 for Eucalyptus and 0.59 for monsoon rainforest. Matasci et al. (2018a) used RF-predicted forest height metrics, with an R^2 ranging between 0.62 and

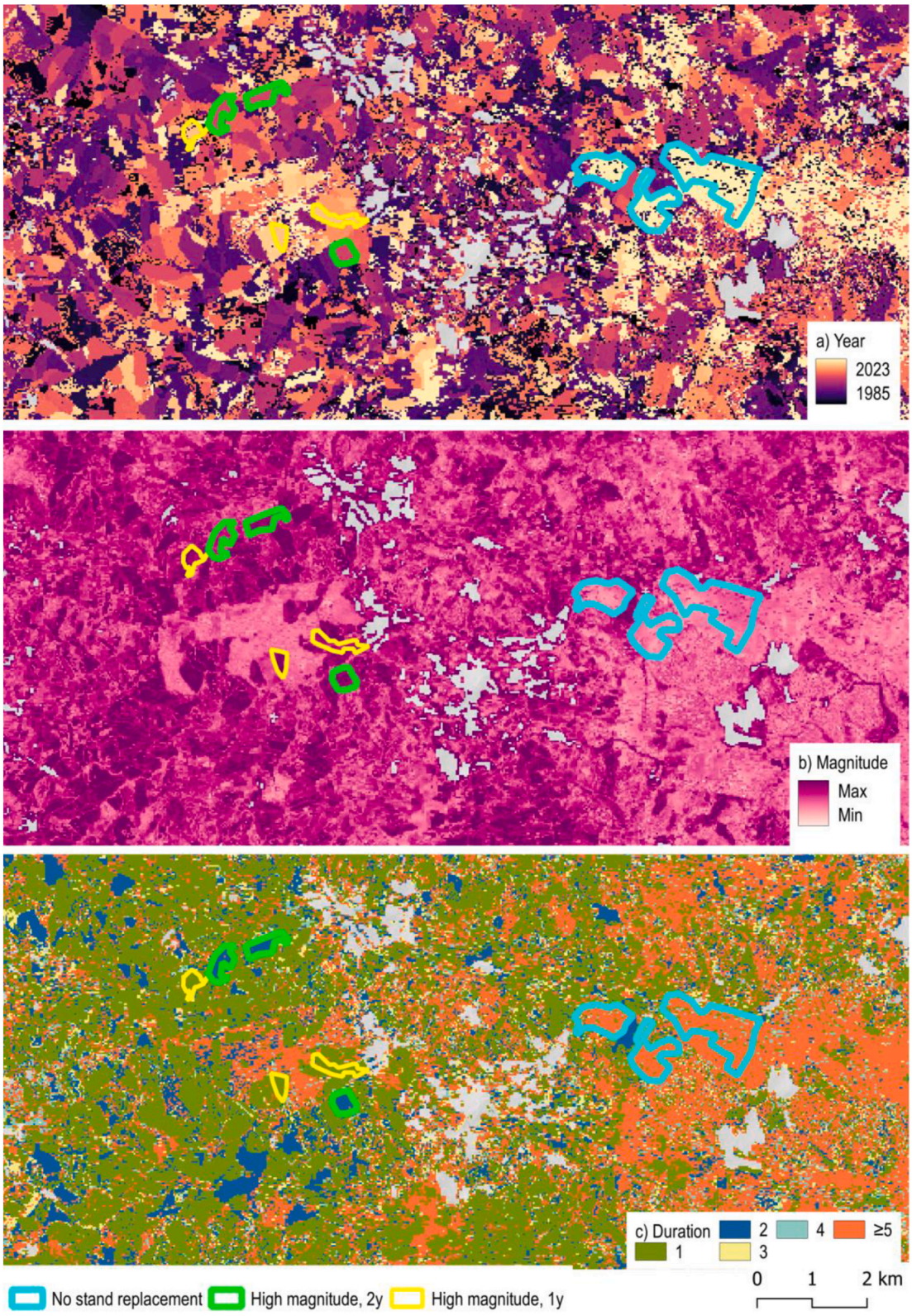

Fig. 4. Example maps of three forest change metrics (see Annex A for a comprehensive overview of the metrics we calculated). The top, central, and bottom panels show, respectively, the year, the magnitude, and the duration of the greatest disturbance that occurred over the study period. Blue polygons are examples of low-magnitude disturbances with a duration greater than five years. Green and yellow polygons are examples of forest harvestings with two and one year of duration, respectively. Such forest change metrics, and the others presented in Annex A – e.g. the number of years since the last disturbance - are significantly correlated with forest height metrics and forest structure variables such as GSV and BA (Matasci et al., 2018).

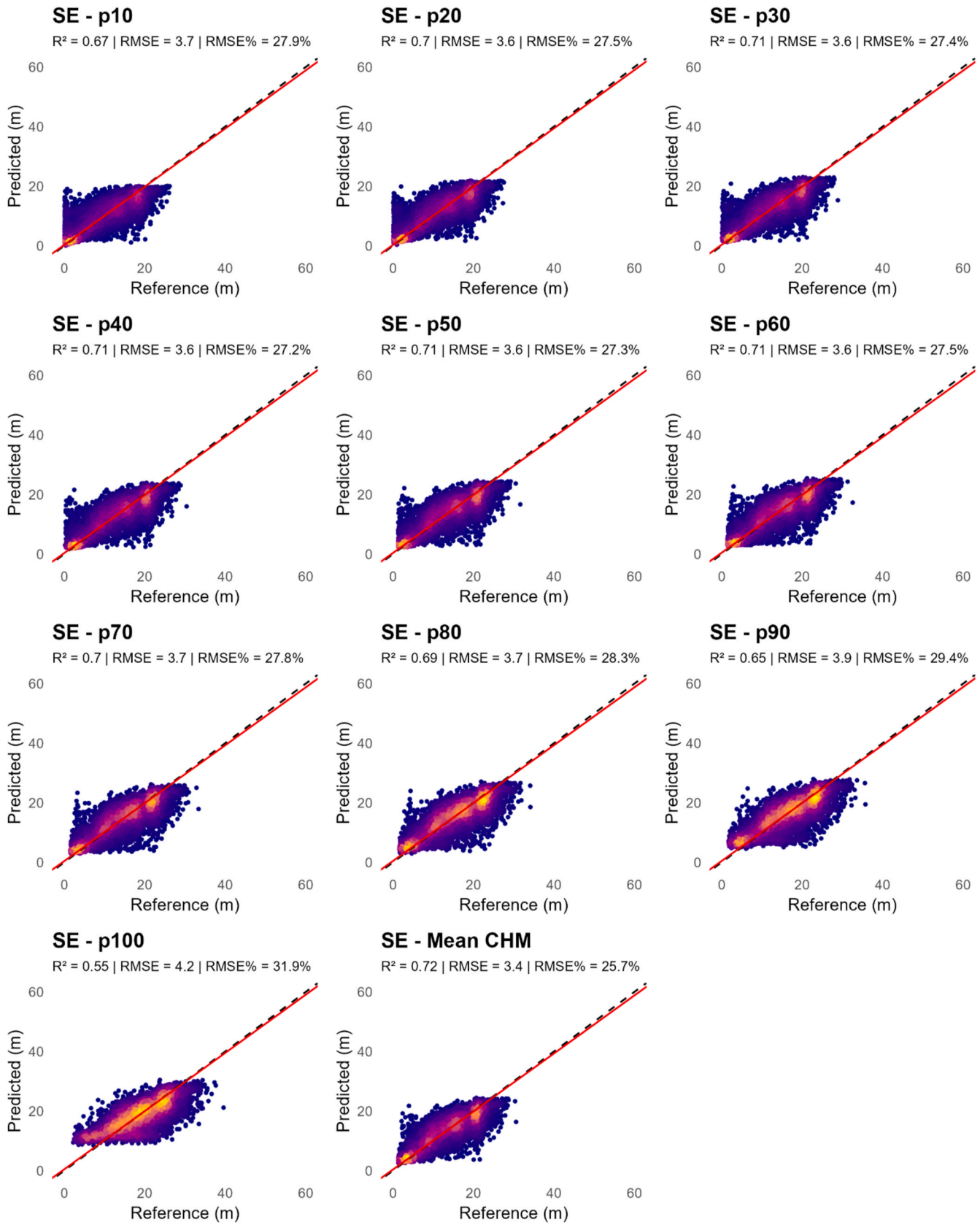

Fig. 5. Performance of the model predicting height metrics statistics in the Vindelälven-Juhttátahkka Biosphere Reserve. Mean CHM is the average of CHM values within ALS plots, while other panels show different percentiles. Yellow and violet dots indicate, respectively, large and low data point density.

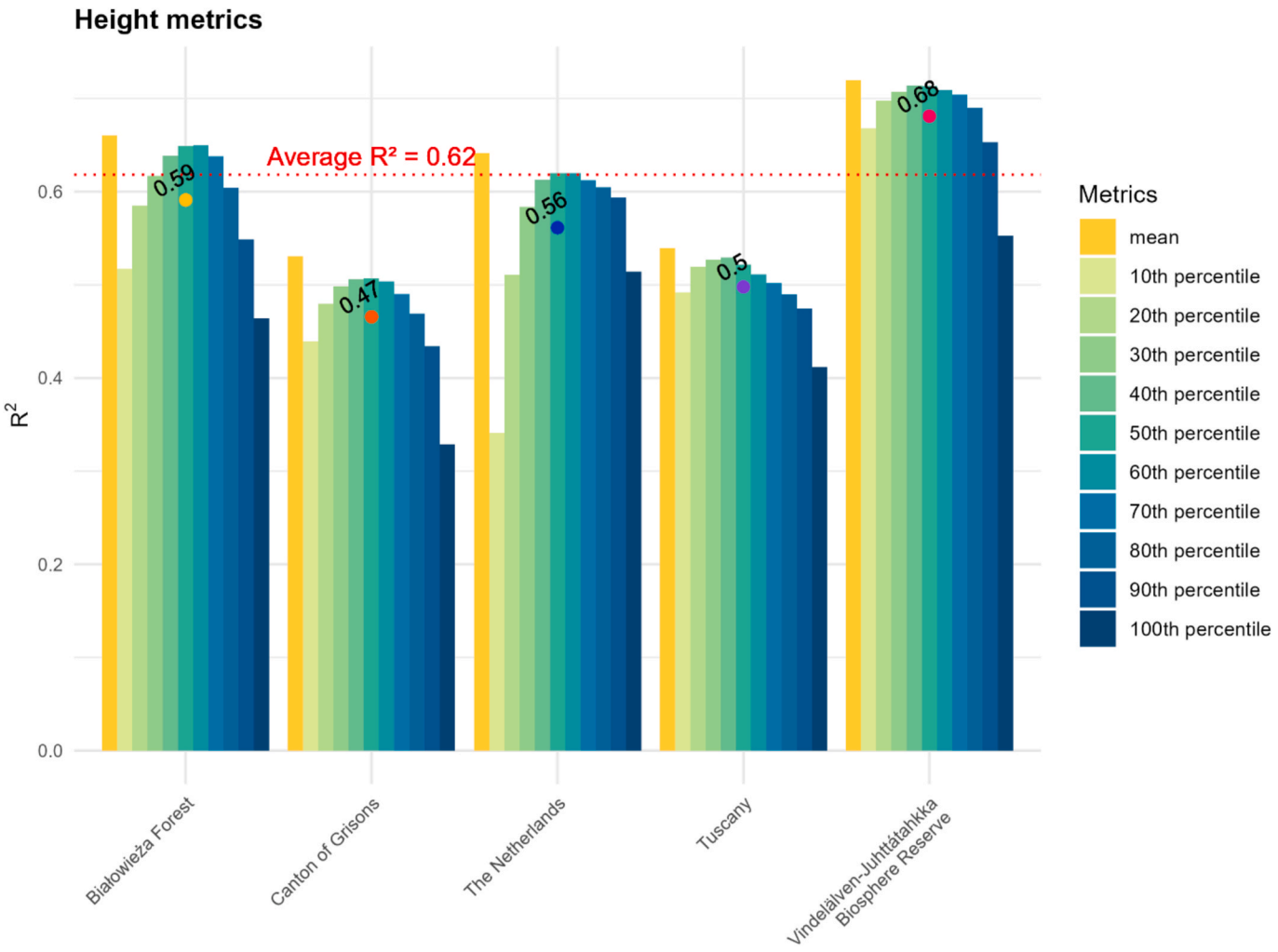

Fig. 6. Summary of height metrics prediction performance. For each height metric and study area, the correlation (in terms of R^2) between prediction and real value is shown. The colored dots show the average R^2 for each study area.

0.64, while Matasci et al. (2018b) predicted key forest attributes with an R^2 ranging between 0.49 and 0.62; however, for some areas (Atlantic Maritime and Taiga Shield West ecozones), the R^2 was lower than 0.3. Coops et al. (2021) reviewed a wide range of studies on methods for estimating forest attributes from LiDAR data across space and time. They reported substantial variation in predictive performance, with R^2 values ranging from 0.38 to 0.90 for forest height metrics and from 0.25 to 0.72 for growing stock volume (GSV). However, only a small subset of these studies used Landsat data, and most were conducted at local scales with highly specific and often non-replicable datasets. Importantly, any of the studies mentioned exploit MTL.

Our approach relies on FCNNs and Landsat time series to provide harmonized predictions of, first, forest height metrics as acquired by ALS and, second, of BA and GSV. Although the characteristics of the input CHMs and the accuracy of the prediction of ALS-derived height metrics vary consistently across the five European study areas (Annex B), this intermediate step was not the final target but part of a broader strategy to infer key forest variables from optical satellite data. (Fogel et al., 2024; Schwartz et al., 2023; Miettinen et al., 2025). Importantly, while our study was structured as five independent case studies to evaluate model transferability across heterogeneous conditions, future research may explore the integration of these datasets for cross-site calibration and to better capture continental-scale patterns (Lang et al., 2022; Tolan et al., 2024).

The combined use of optical satellite and ALS data enables broader applications across various forest types and geographic regions, as our results over very different regions and forests indicate. However, challenges remain, particularly in areas with persistent cloud cover or steep slopes, which can degrade the quality of optical data and ALS acquisitions (D'Amico et al., 2021b). Future efforts should focus on optimizing algorithms, such as BAP compositing, and integrating additional data sources (e.g., Sentinel satellites) to address these challenges. Further, the herein presented model would benefit from a more in-depth analysis and automated classification of the different forest disturbances occurring across Europe and in our study areas, as they affect biomass and forest three-dimensional structure heterogeneously. Herein, several predictors of disturbances and recovery were provided to the model to try to infer the different impacts that diverse disturbance types may have; however, further effort may improve the outcomes. Critically, the quality of ALS data can be poor, especially in older datasets with lower resolution or outdated acquisition techniques. For example, the lower accuracy observed in Tuscany was attributed to the age (2008) and quality (average point density of 1.6) of ALS data used for training (Table 2). Similarly, complex terrain and high variability in tree height, as seen in Switzerland, pose more challenges for accurate modeling. Additionally, Landsat data and acquisition frequency limit the temporal resolution of predictions to a yearly basis. While the methodology effectively utilizes all available Landsat data, future improvements could incorporate higher-resolution datasets from newer satellites (e.g., Sentinel-2) to improve precision in complex environments and the frequency of data

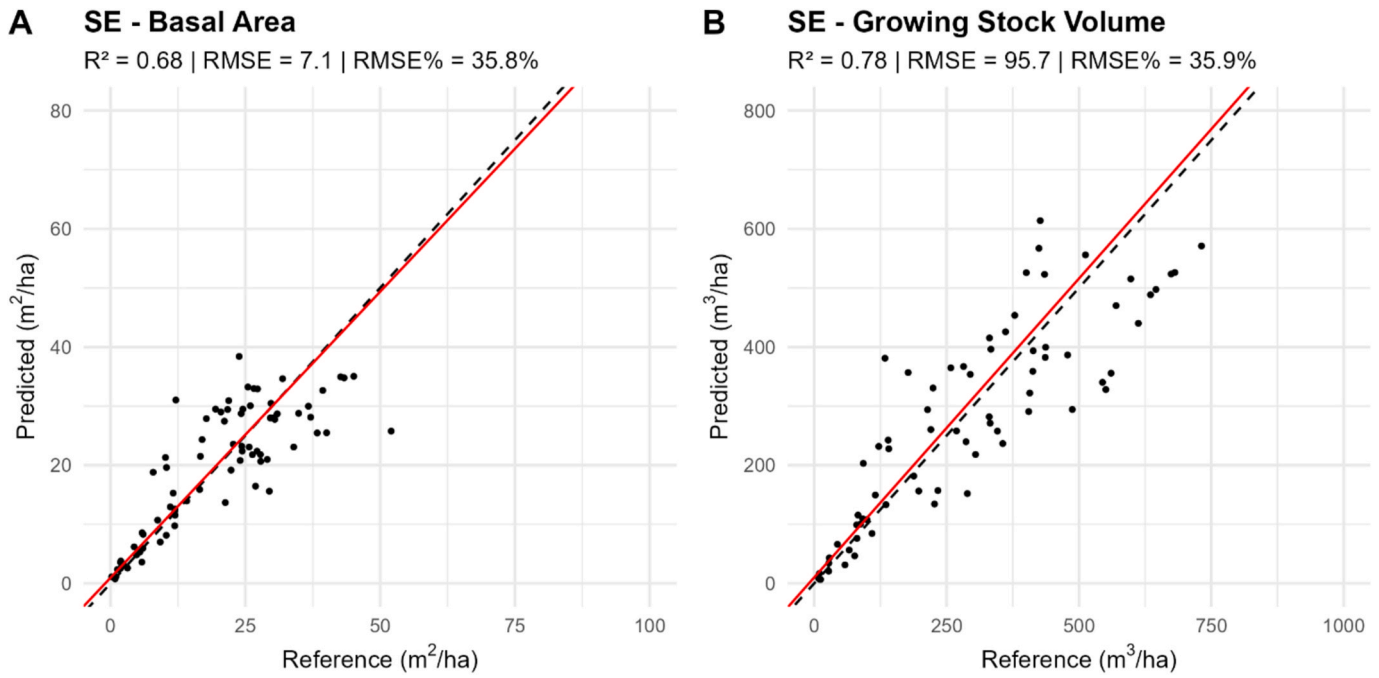

Fig. 7 –. R^2 and RMSE of predicted GSV and BA, within the Vindelälven-Juhttátahkka Biosphere Reserve.

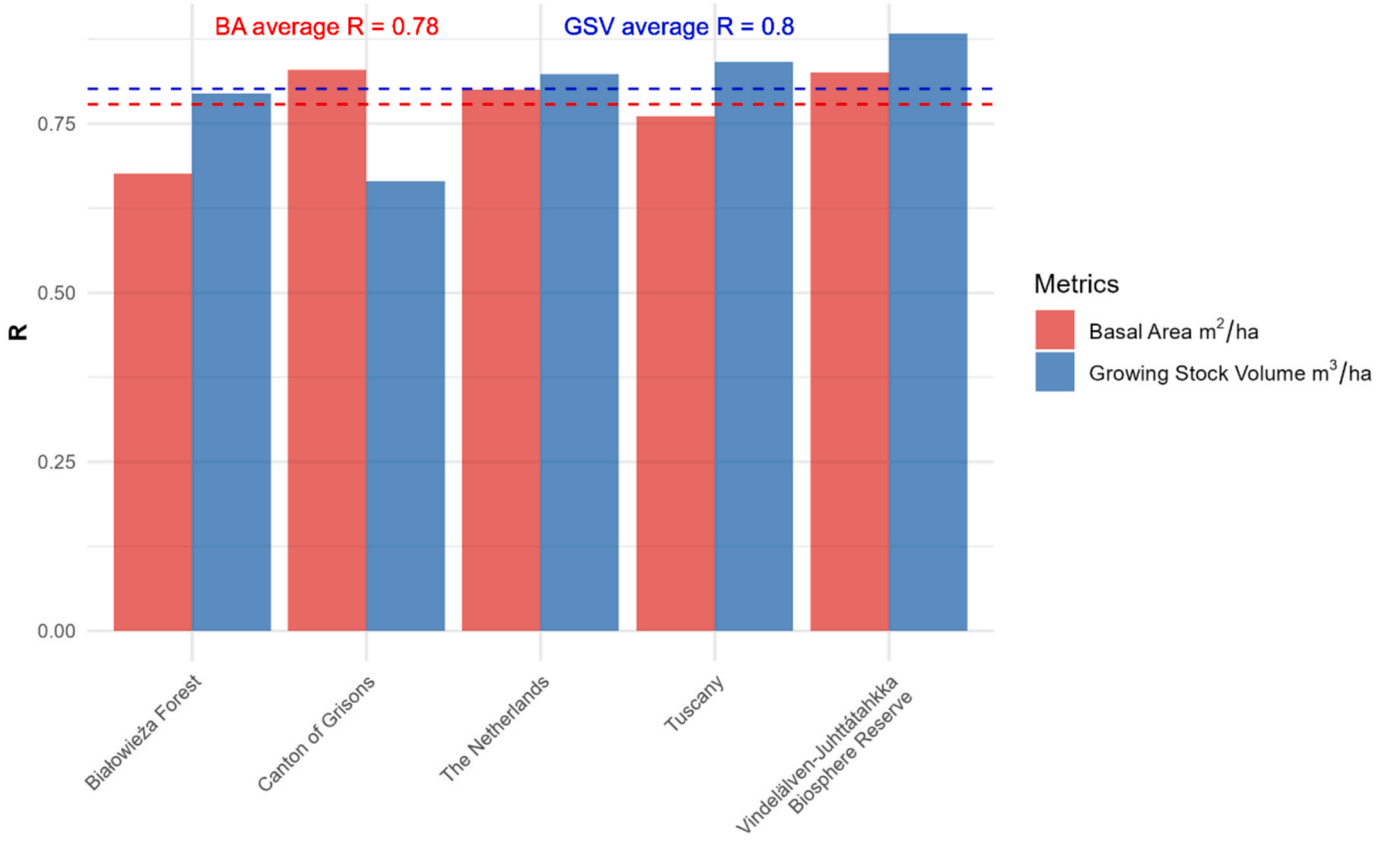

Fig. 8. – Summary of the R^2 reached in the five study areas for GSV and BA.

updates (D'Amico et al., 2022; Francini et al., 2020; Fassnacht et al., 2024; Gregoire et al., 2016).

In this study, the uncertainty of the final predictions was assessed by independent validation using field data. Such validation can be a valuable strategy for assessing uncertainty and comparing it with other methods. However, what is critical when using information in decision making, e.g., in forest management, or in policy formulation, is the uncertainty of the predictions of every individual pixel if the spatial map representation is important, or more importantly, the uncertainty of predictions (estimates) for larger areas of interest. Such areas can be

management domains, provinces, nations, or even the entire continent, depending on context. The uncertainty of such predictions can hardly be inferred from the current analysis. The current application does not assume any particular sampling design underlying the collection of field data used to train the models. For the future application of the proposed methodology, it is reasonable to assume that probabilistic field samples will be unavailable, and an opportunistic strategy for accessing field training data will be the most realistic option. This means that solutions to the inferential problem must be found within the realm of model-based inference. For non-parametric techniques such as neural networks, analytically derived, closed-form estimators of variance do not exist. Resampling techniques, such as bootstrapping, have garnered substantial interest in recent years within the remote sensing community and have shown great promise for statistically rigorous inference in natural resource estimates, including biomass and GSV (e.g., Esteban et al., 2019; McRoberts et al., 2022). It may be computationally challenging to apply bootstrapping to large spatial domains, as tens of thousands, or even more, full replications of the entire modeling and prediction chain may be required to achieve stabilization of the estimates (McRoberts et al., 2023). The computational challenge may become even more complicated if the modeling and prediction chain involves several subsequent steps, as in this study, each of which induces uncertainty that propagates through the chain to the final estimates. Recent research may suggest viable solutions even to that challenge. In a recent study by Saarela et al. (2025) it was demonstrated for a hierarchical inferential problem with two separate and subsequent models that the computations could be divided into separate parts. A key effort in further developing methodologies, such as those proposed in the current study, should focus on providing complete and statistically rigorous inference, including methods for handling the computational burden in complex, multi-step applications.

7. Conclusions

This study demonstrates a comprehensive and integrated methodology using Landsat data and disturbance and recovery predictors to derive forest height metrics and key forest variables by relying on multi-task FCNNs, which are capable of predicting multiple variables at once. The herein introduced approach demonstrates the potential for integrating various data sources to facilitate more advanced forest monitoring, addressing gaps in ALS data availability, and providing scalable methods for predicting forest structure over large areas. The approach is intended to complement the scarcity of ALS data availability, providing a solution for covering estimated ALS data in those European areas where frequent updates of ALS data are not available. Indeed, to overcome the challenge of inconsistent ground-based data availability, this study demonstrated the pivotal role that the effective integration of satellite optical and ALS data could play. The novel approach of integrating partial ALS data with wall-to-wall Landsat data via multi-task FCNN establishes a replicable methodology that can be expanded to predict additional key forest attributes to GSV and BA, such as those relevant to biodiversity or those that support the classification of forest types. The approach can be considered generalizable, as the experiment was conducted in five areas with very different forests and biogeographic conditions, and the model achieved high accuracies in all of them. Additionally, several parameters and thresholds of our algorithms can be adjusted and adapted to accommodate varying imagery availability due to cloud coverage, different characteristics of forest ecosystems, and types of forest disturbance.

In conclusion, this study demonstrates the feasibility of integrating satellite and ALS data with ground observations to produce reliable, scalable forest structure estimates. The approach supports key forest management decisions by enabling consistent and timely monitoring across diverse European landscapes. It offers a concrete step toward the development of an operational, harmonized forest monitoring framework at the continental scale.

CRediT authorship contribution statement

Saverio Francini: Writing – review & editing, Writing – original draft, Resources, Data curation, Conceptualization. **Costanza Borghi:** Writing – review & editing, Visualization. **Giovanni D'Amico:** Writing – review & editing, Data curation. **Lars T. Waser:** Writing – review & editing. **Maciej Lisiewicz:** Writing – review & editing, Data curation. **Krzysztof Stereńczak:** Writing – review & editing, Data curation. **Mart-Jan Schelhaas:** Writing – review & editing, Data curation. **Cameron Pellett:** Writing – review & editing, Data curation. **Terje Gobakken:** Writing – review & editing. **Erik Næsset:** Writing – review & editing, Validation. **Federico Magnani:** Writing – review & editing. **Sergio de-Miguel:** Writing – review & editing. **Gert-Jan Nabuurs:** Writing – review & editing, Resources. **Ruben Valbuena:** Writing – review & editing, Resources. **Gherardo Chirici:** Writing – review & editing, Resources.

Declaration of competing interest

The authors declare that they have no known competing financial interests or personal relationships that could have appeared to influence the work reported in this paper.

Acknowledgements

•EFINET "European Forest Information Network" funded by the European Forest Institute, Network Fund G-01-2021.

•FORWARDS. H2020 project funded by the European Commission, number 101084481 call HORIZON-CL6-2022-CLIMATE-01-05.

•SUPERB. H2020 project funded by the European Commission, number 101036849 call LC-GD-7-1-2020.

•MONIFUN. H2020 project funded by the European Commission, number 101134991 call HORIZON-CL6-2023-CircBio-01-14.

•NextGenCarbon. H2020 project funded by the European Commission, number 101184989 call HORIZON-CL5-2024-D1-01-07.

•PNRR, funded by the Italian Ministry of University and Research, Missione 4 Componente 2, "Dalla ricerca all'impresa", Investimento 1.4, Project CN00000033.

•MULTIFOR "Multi-scale observations to predict Forest response to pollution and climate change" PRIN 2020 Research Project of National Relevance funded by the Italian Ministry of University and Research (prot. 2020E52THS)

• ALS acquisition and plot data collection from Białowieża Forest was supported by Project LIFE + ForBioSensing (contract number LIFE13-ENV/PL/000048) and Poland's National Fund for Environmental Protection and Water Management (contract number 485/2014/WN10/OPNMLF/D). The work was also supported by internal funds under project "AFTER FBS - maintenance of ForBioSensing project performance indicators" (internal no. 261509) and "Assessment and monitoring of changes in the state of biodiversity in the Białowieża Forest based on selected natural elements – continuation" project financed by the State Forests National Forest Holding (contract number MZ.271.July 3, 2022, internal no. 500483)

• The Dutch NFI is funded by the Ministry Agriculture, Nature Management and Food Quality. We thank the steering group of the NFI for their support. The NFI is carried out by WENR together with Probos, Borgman and van Nierop

•The Swiss National Forest Inventory (NFI) is a cooperative effort between the Swiss Federal Institute for Forest, Snow and Landscape Research (WSL) and the Swiss Federal Office for the Environment (FOEN). The LiDAR data was provided by swisstopo and WSL.

Annex A.

Table 1
Set of predictors used for the analysis, consisting of six spectral bands, seven vegetation indices, 33 change metrics, and image acquisition day of year (DOY) calculated using the BAP method (Section 4.1)

n	Predictors	Description	Reference
6	**a. Spectral Bands**		
1	blue	Blue band	
2	green	Green Band	
3	red	Red band	
4	nir	Near Infrared band	
5	swir1	Shortwave Infrared 1 band	
6	swir2	Shortwave Infrared 2 band	
1	**DOY**	Day of the year - Date of acquisition of observed pixel	Griffiths et al. (2013)
7	**b. Vegetation indexes**		
1	EVI	Enhanced Vegetation Index – Optimizes vegetation signal in high biomass regions.	(Huete et al., 2002)
2	NBR	Normalized Burn Ratio – Highlights burned areas and differentiates burn severity	Key and Benson (2006)
3	NDVI	Normalized Difference Vegetation Index – Measures vegetation health through light reflection	(Huang et al., 2021)
4	TCA	Tasseled Cap Angle - Arc tangent formed by Greenness and Brightness	Crist and Cicone (1984)
5	TCB	Tasseled Cap Brightness – Reflects overall brightness, sensitive to soil	
6	TCG	Tasseled Cap Greenness – Sensitive to vegetation abundance	
7	TCW	Tasseled Cap Wetness – Sensitive to soil and plant moisture	
33	**c. Change Metrics**		
1	nVertices	Number of segmented vertices	Kennedy et al. (2010)
2	yearsToPreviousVertex	Year to precedent segmented vertex	
3	yearsToSubsequentVertex	Year to subsequent segmented vertex	
4	greatestDisturbanceMagnitude	Magnitude value of the greatest disturbance	
5	greatestDisturbanceYear	Year of the greatest disturbance	
6	preChange_blue	Blue band value of the last disturbance occurred	
7	preChange_green	Green band value of the last disturbance occurred	
8	preChange_red	Red band value of the last disturbance occurred	
9	preChange_nir	NIR band value of the last disturbance occurred	
10	preChange_swir1	SWIR1 value of the last disturbance occurred	
11	preChange_swir2	SWIR2 value of the last disturbance occurred	
12	preChange_EVI	EVI value of the last disturbance occurred	
13	preChange_NBR	NBR value of the last disturbance occurred	
14	preChange_NDVI	NDVI value of the last disturbance occurred	
15	preChange_TCA	TCA value of the last disturbance occurred	
16	preChange_TCB	TCB value of the last disturbance occurred	
17	preChange_TCG	Last pre-disturbance TCG value	
18	preChange_TCW	TCW value of the last disturbance occurred	
19	preChange_doy	Doy of the last disturbance occurred	
20	postChange_blue	Post-disturbance Blue band	
21	postChange_green	Post-disturbance Green band	
22	postChange_red	Post-disturbance Red band	
23	postChange_nir	Post disturbance NIR	
24	postChange_swir1	Post-disturbance SWIR1 band	
25	postChange_swir2	Post-disturbance SWIR2 band	
26	postChange_EVI	Post-disturbance EVI	
27	postChange_NBR	Post-disturbance NBR	
28	postChange_NDVI	Post-disturbance NDVI	
29	postChange_TCA	Post-disturbance TCA	
30	postChange_TCB	Post-disturbance TCB	
31	postChange_TCG	Post-disturbance TCG	
32	postChange_TCW	Post-disturbance TCW	
33	postChange_doy	Day of the year of post-disturbance pixel	

Annex B.

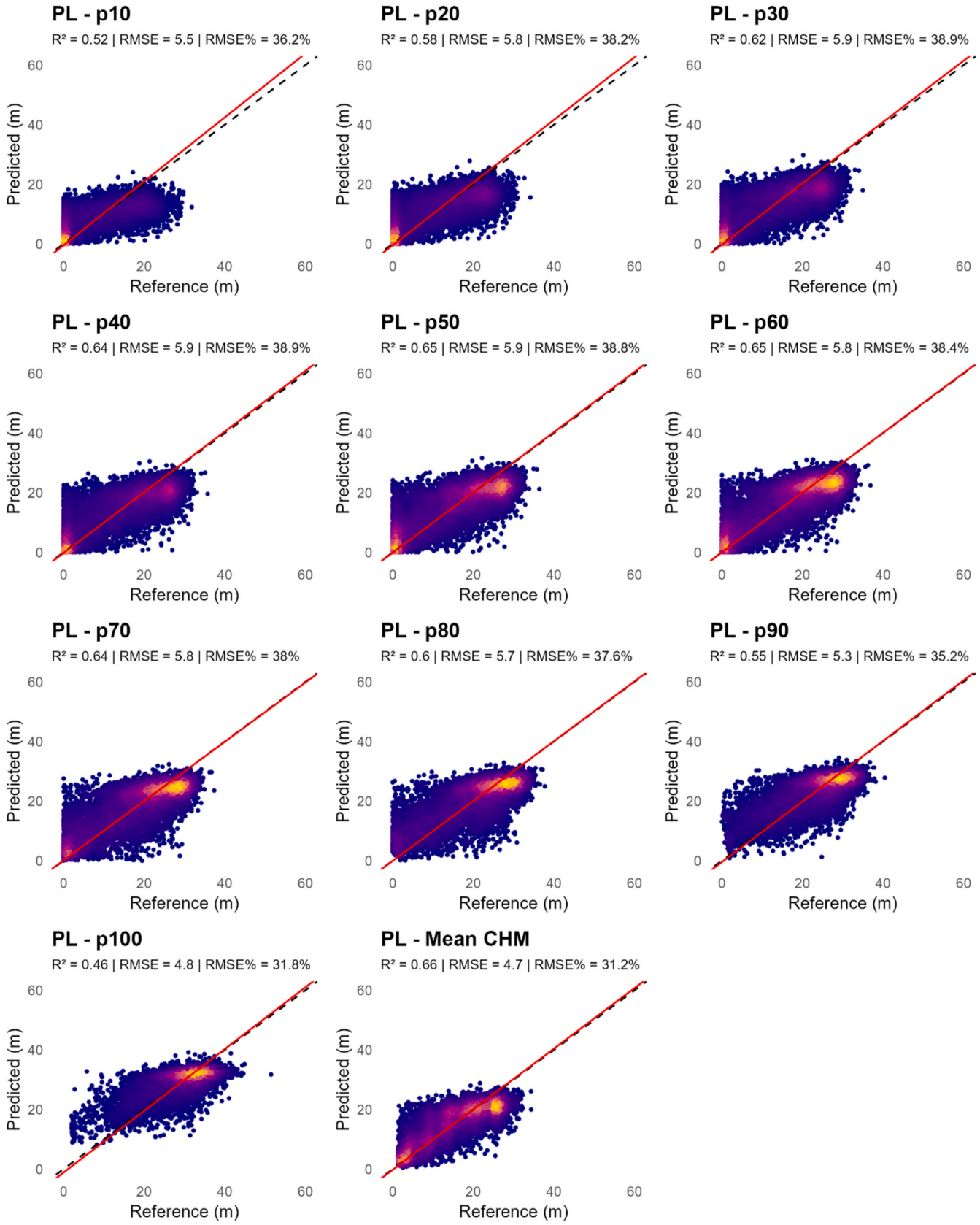

Fig. 1b. Performance of the model predicting height metrics statistics in Białowieża Forest (PL).

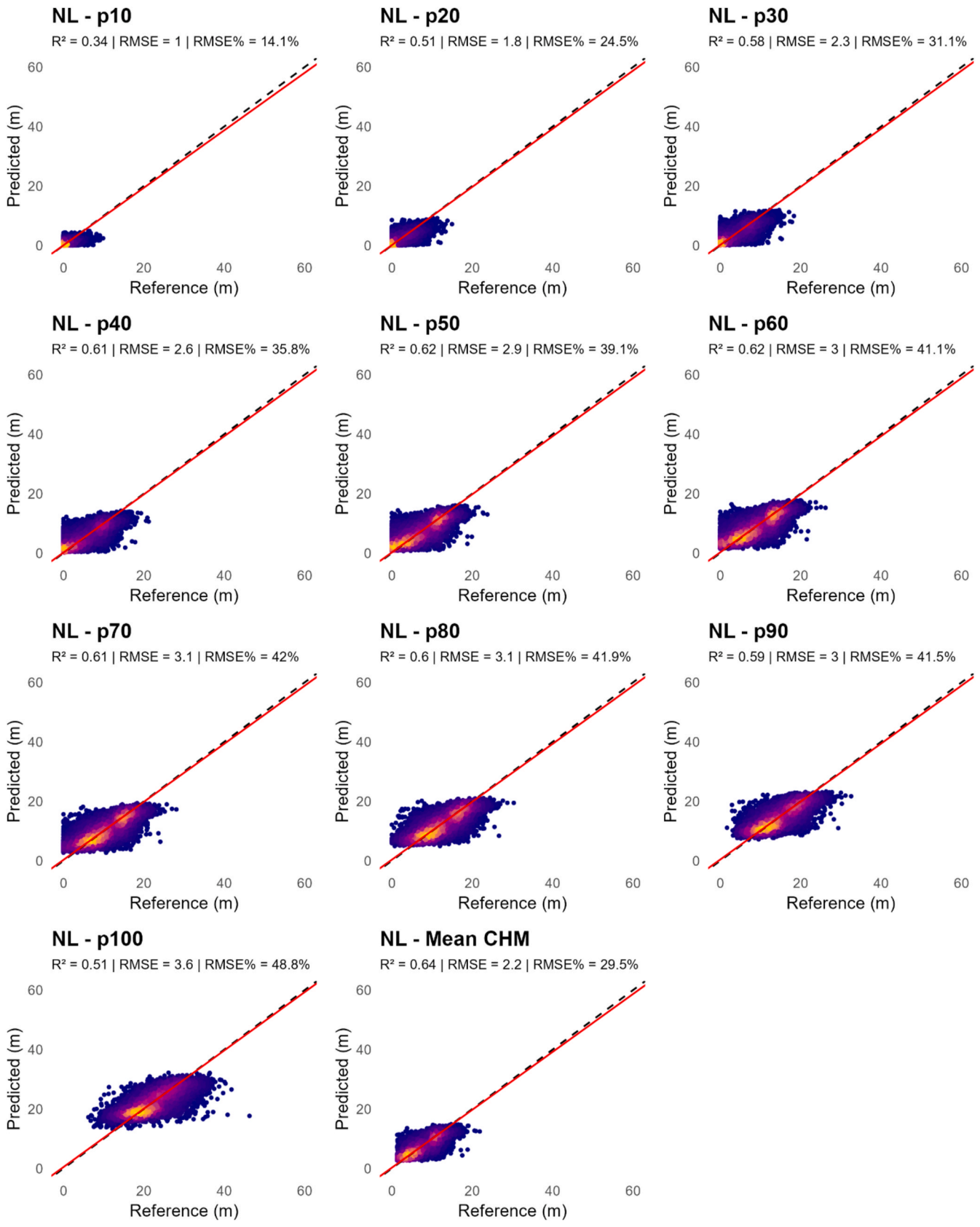

Fig. 2b. Performance of the model predicting height metrics statistics in The Netherlands.

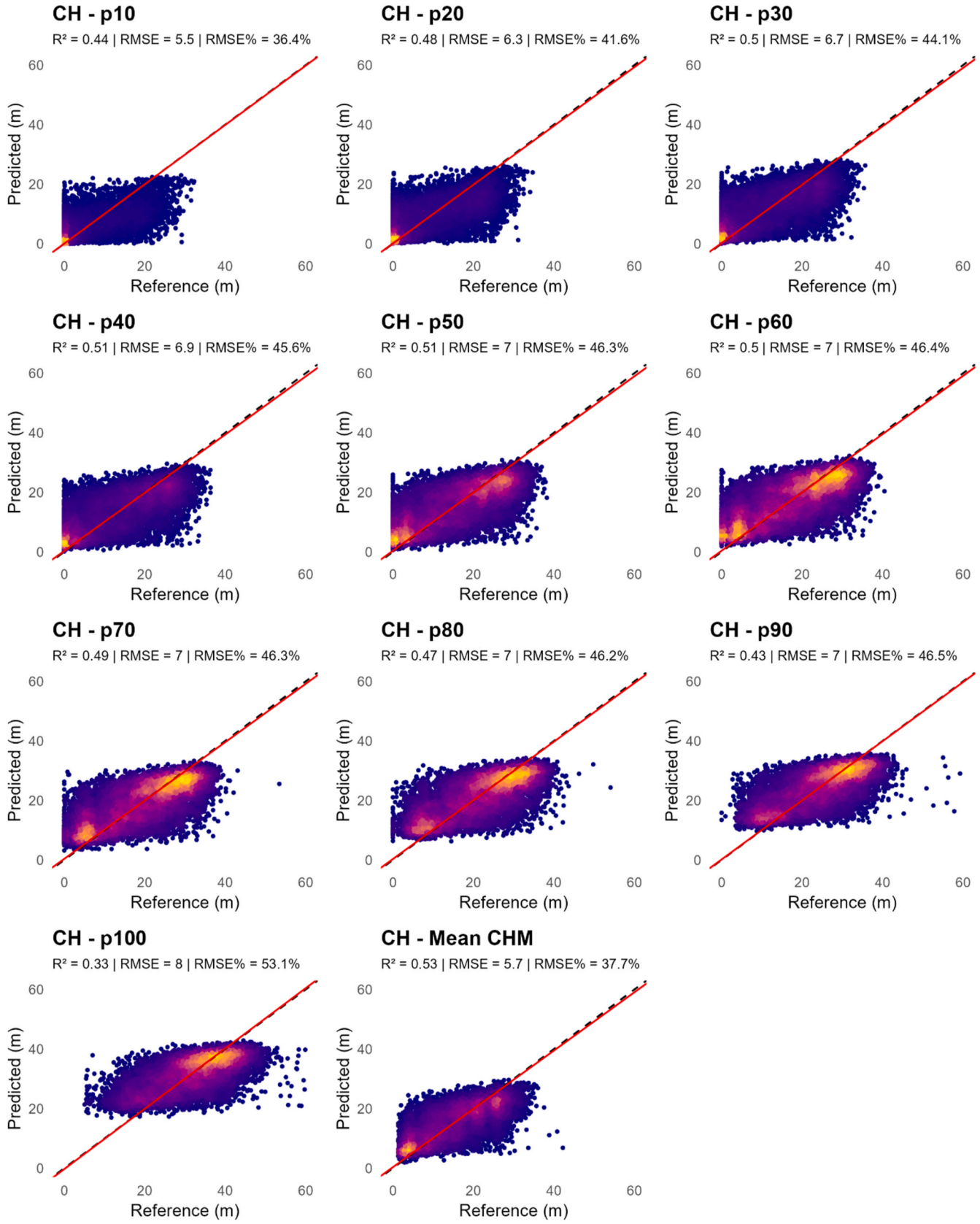

Fig. 3b. Performance of the model predicting height metrics statistics in the Canton of Grisons (CH).

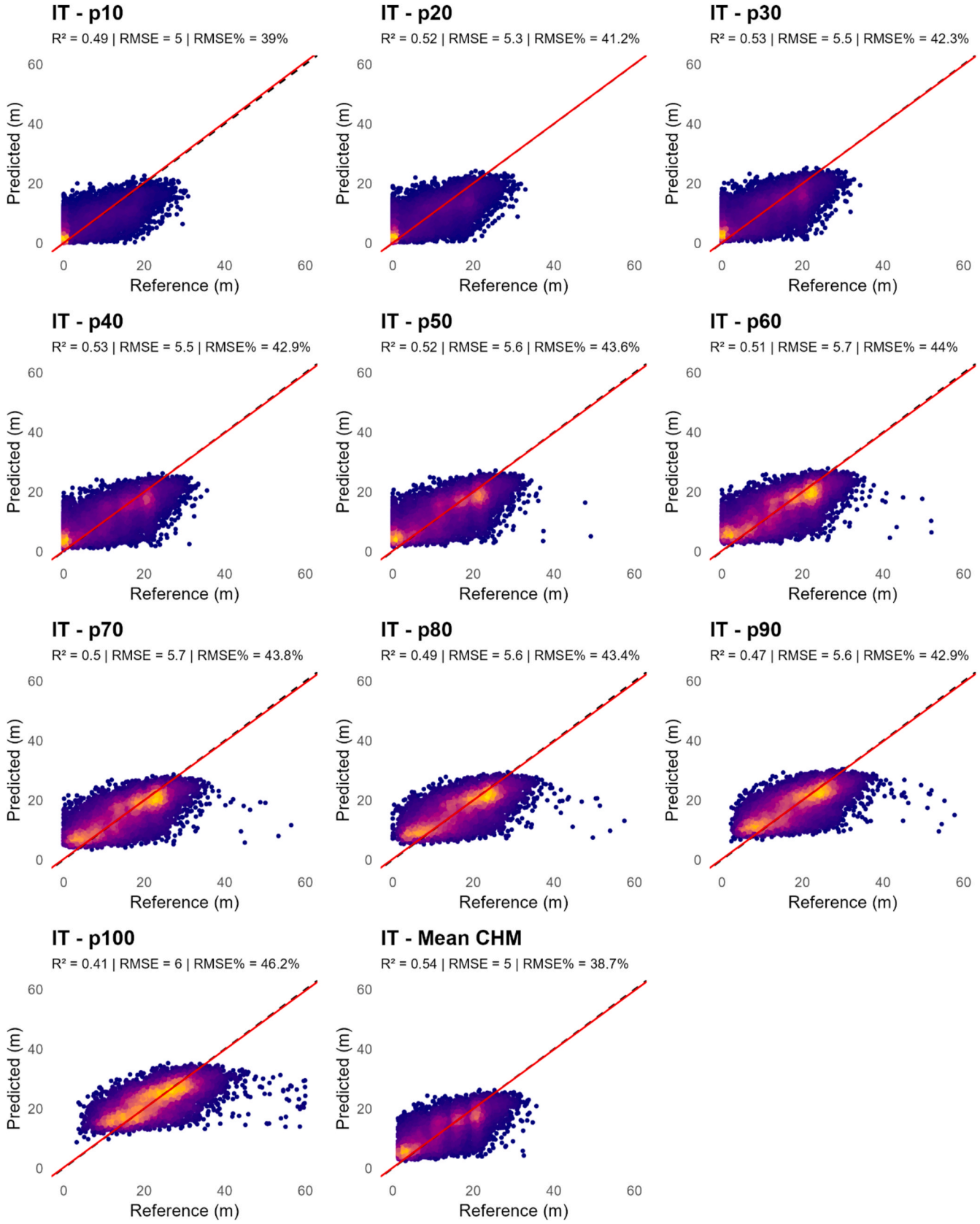

Fig. 4b. Performance of the model predicting height metrics statistics in Tuscany (IT).

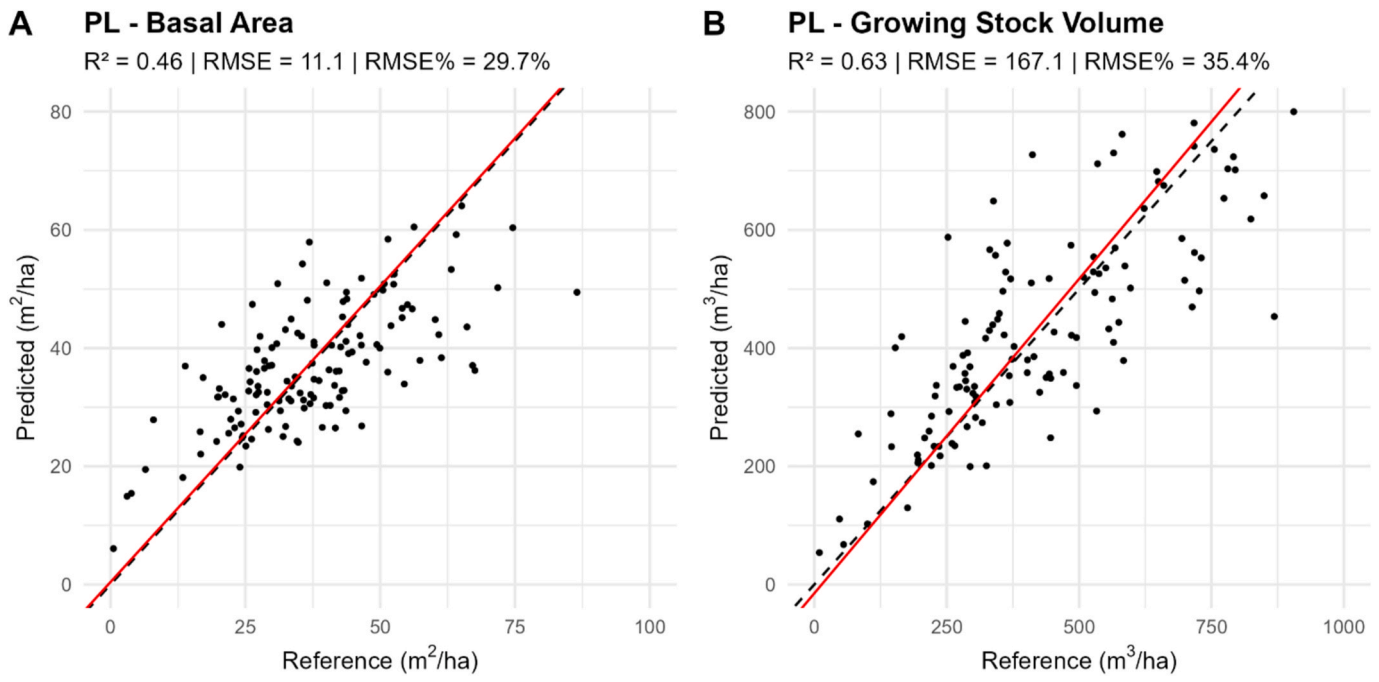

Fig. 5b. Pearson correlation coefficient (R^2) and root mean square error (RMSE) calculated (independently) on predicted growing stock volume and basal area, within the Polish study area (Białowieża Forest).

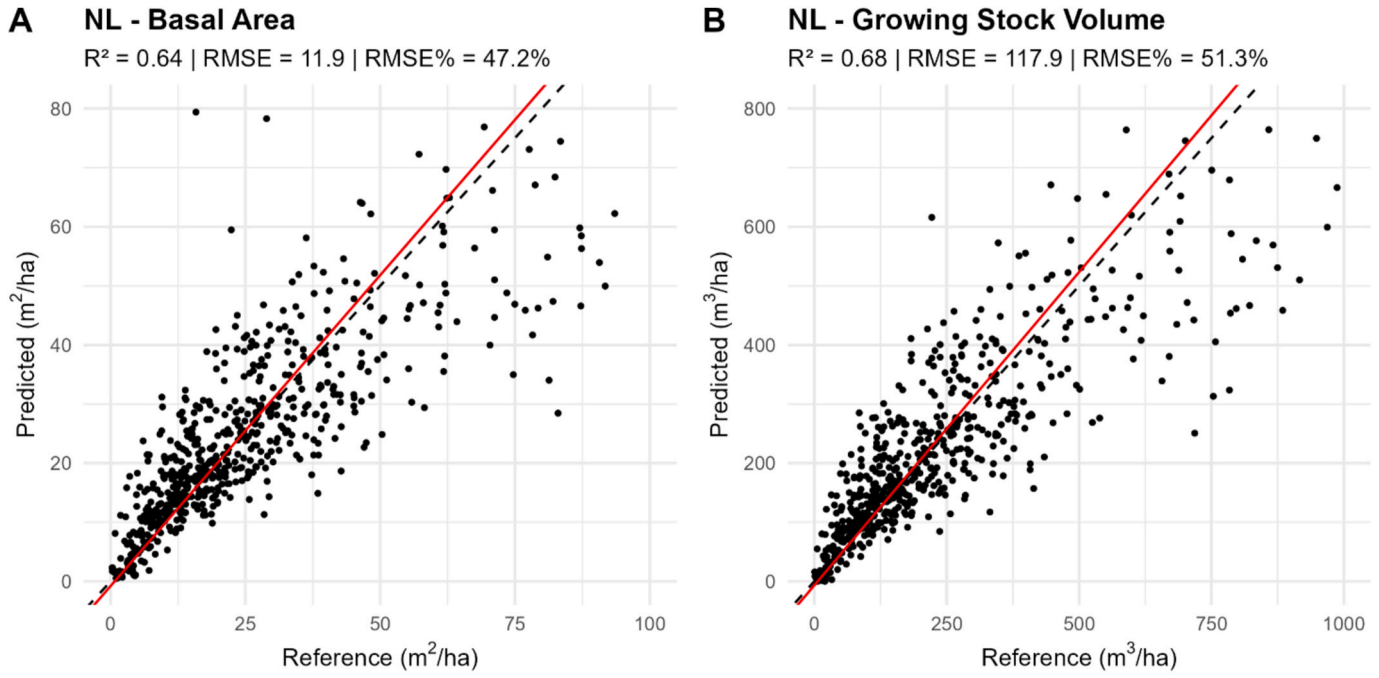

Fig. 6b. Pearson correlation coefficient (R^2) and root mean square error (RMSE) calculated (independently) on predicted growing stock volume and basal area, within the Dutch study area.

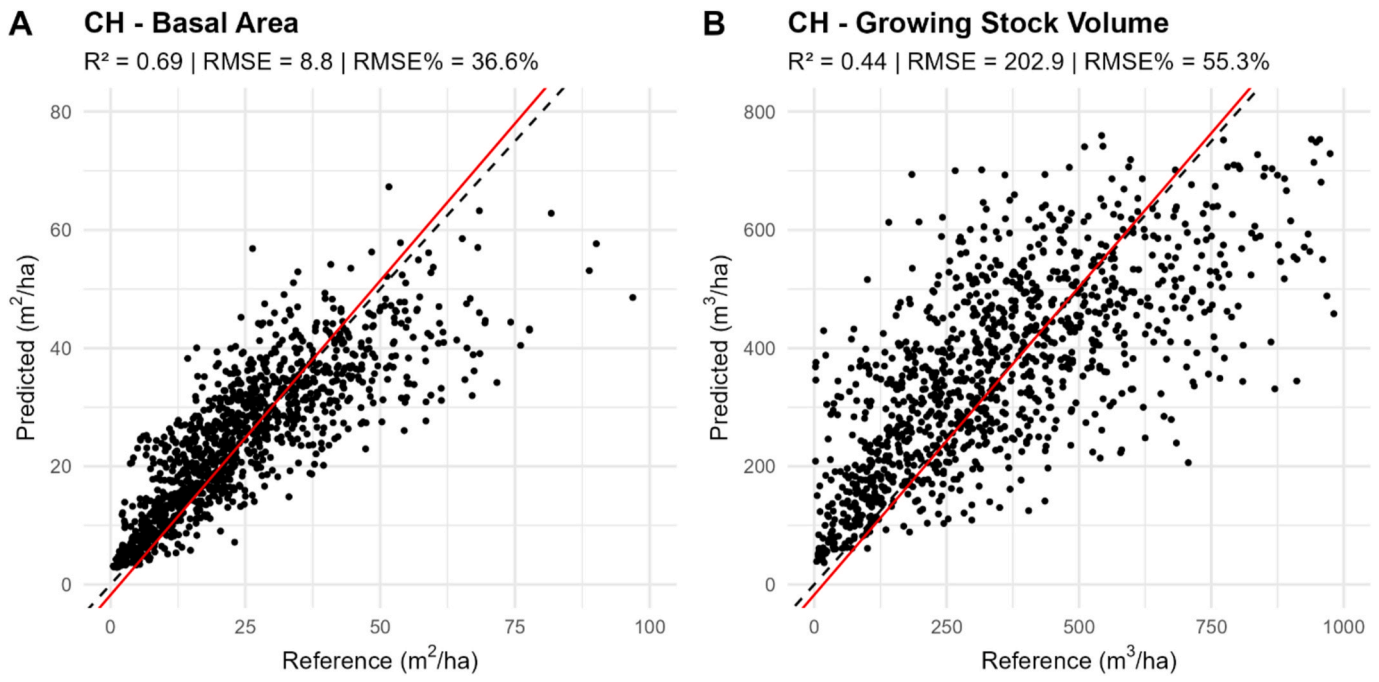

Fig. 7b. Pearson correlation coefficient (R^2) and root mean square error (RMSE) calculated (independently) on predicted growing stock volume and basal area, within the Swiss study area (Canton of Grisons).

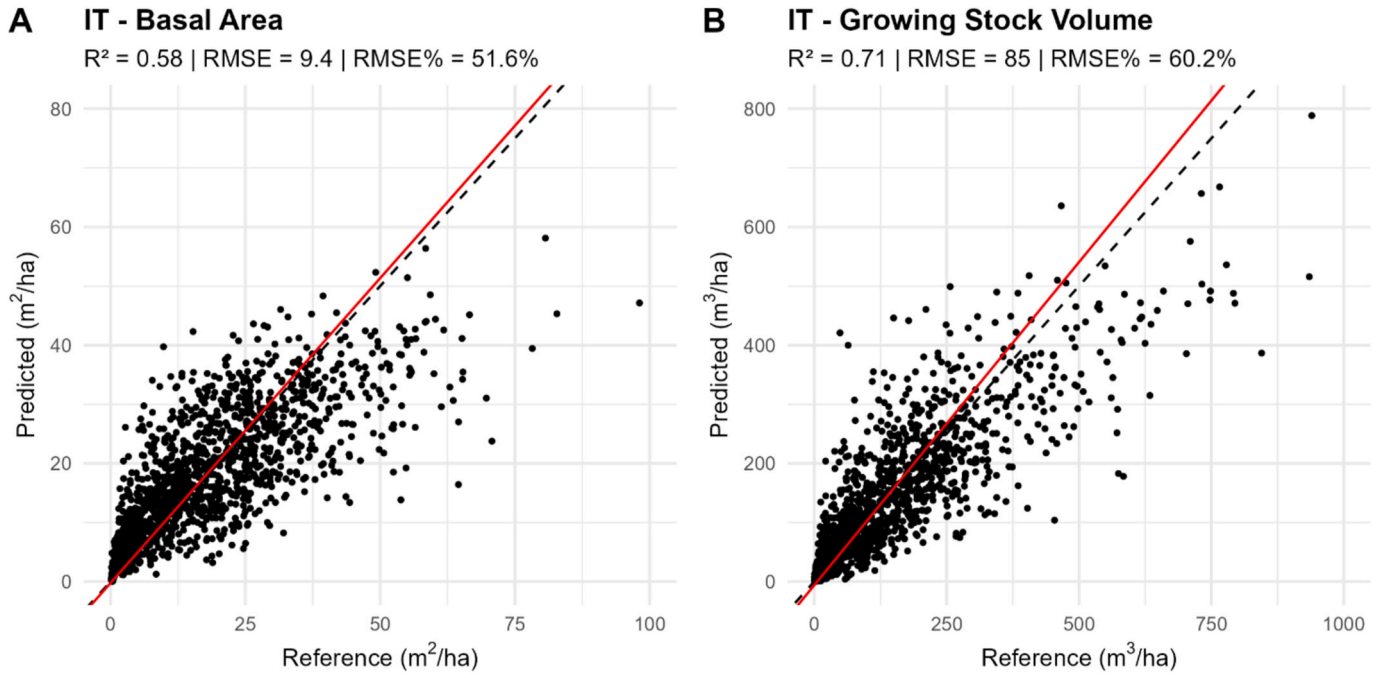

Fig. 8b. Pearson correlation coefficient (R^2) and root mean square error (RMSE) calculated (independently) on predicted growing stock volume and basal area, within the Italian study area (Tuscany).

Annex C.

Table C.1
Input parameters needed to (i) calculate BAP (best available pixel) composites, (ii) remove noise from composites, and (iii) apply temporal segmentation to predict and characterize forest changes

Input parameters	Białowieża Forest, PL	The Netherlands	Canton of Grisons CH	Tuscany, IT	Vindelälven-Juhttátahkka Biosphere Reserve, SE
BAP - Best Available Pixel					
Start year	1984	1984	1984	1984	1984
End year	2022	2022	2022	2022	2022
Target day	07–01	07–01	07–15	08–01	08–01
Day range	60	60	45	30	30
Cloud threshold	50	70	70	70	70
SLC off penalty	0.3	0.3	0.3	0.3	0.3
Opacity score min	0.2	0.2	0.2	0.2	0.2
Opacity score max	0.3	0.3	0.3	0.3	0.3
Cloud distance max	1500	1500	1500	1500	1500
Remove noise					
Despike band threshold	0.65	0.65	0.65	0.65	0.65
Despike n° bands	3	3	3	3	3
Temporal segmentation					
Index	NBR	NBR	NBR	NBR	NBR
Despike index threshold	0.85	0.85	0.85	1	1
Max segments	7	7	7	7	7
Max error	45	45	45	45	45
Minimum Mapping Unit	5	5	5	5	5

Annex D.

D.1 Vindelälven-Juhttátahkka Biosphere Reserve

Swedish NFI plots that intersected with the study area, the Vindelälven-Juhttátahkka Biosphere Reserve, were selected as field reference data. The Swedish NFI design for the study region utilizes randomized sampling of a 5 km spaced grid of potential sampling positions (Fridman et al., 2014). For each selected position, clusters of 12 or 8 sampling plots with a 7- or 10-m radius are then surveyed for temporary (sampled only once) and permanent (returned to every 5 years) plots, respectively. Each cluster of plots, or so-called tract, is arranged in a rectangle with variable side lengths depending on the homogeneity of the environment in the region, increasing from 300 to 1800 m with increasing homogeneity. Plot centers are located and measured using hand-held GNSS receivers (Garmin GPSMAP 64) providing locations within an accuracy of around 5 m (D'Amico et al., 2024; Nilsson et al., 2017). All trees with a DBH greater than 10 cm are callipered in each plot, then a smaller subplot with a 3.5-m radius is used to measure the remaining trees with a DBH greater than 4 cm. As well as diameters, species, and heights are collected, allowing GSV prediction with allometric regression models (Nilsson et al., 2017).

D.2 Białowieża forest

In the Białowieża forest, 685 monitoring plots were established (in this study, we used 672 plots that contained trees). The monitoring plots have a radius of 12.62 m, representing 500 m^2 of area. The centers of individual plots were accurately measured using a real-time kinematic receiver or a static geodetic class receiver for global navigation satellite systems. The SD = 0.096 m was the result of differential pre-processing of global navigation satellite system data. The plots form the basis for multi-year, comprehensive monitoring of the dynamics of the forest stands. More than a dozen different biometric characteristics of the trees were measured (including height and DBH). Forest regeneration, i.e., the emergence of a new generation of trees, was also inventoried and analyzed. The established monitoring plots represent the entire variability in the habitat and stand conditions of Białowieża Forest. Measurements were taken three times, i.e., in 2015, 2017, and 2019. The fieldwork aimed to determine the condition of the forest stands and to collect comparative (reference) materials for data acquired using remote sensing methods. Data from field measurements are freely available in the Forest Research Institute of Poland.

D.3 The Netherlands

For the Netherlands, NFI data were used as ground reference data. The Dutch NFI design consists of an unaligned systematic grid with one sample plot per 100 ha. Sample plots are circular with a variable radius, such that at least 20 trees are included, limited to a range of 5–20 m. All trees on the sample plot are callipered, their species are recorded as well as their status (alive, dead standing, or dead lying) and social position. In addition, some characteristics of the stand are recorded, including the size class of the stand (<0.1 ha, 01–0.5 ha, >0.5 ha), the main species, and the crown coverage of the tree and the shrub layer. The actual plot coordinates may deviate slightly (maximum 20 m) from the coordinates as given by the original grid map, due to inaccuracies in the GPS measurements used when the sample plots were established in the field.

For this study, we extracted data from the NFI6 (Schelhaas et al., 2014) from the online database (www.probos.nl/publicaties/overige/1094-mfv-2006-nbi-2012), amended with the exact coordinates of the plots. For training purposes, it was important to be sure that the plots and the tree species they contain could unambiguously be linked to the spectral signal. We therefore limited our selection to plots for which the main recorded species on the plot had a BA share of at least 80 % and was equal to the main species of the stand. Species on the plot may deviate from the main species

of the stand due to the presence of groups of admixed species. This resulted in a set of 1398 sample plots with suitable training data.

D.4 Canton of Grisons, Switzerland

The Swiss NFI is a continuous inventory comprising approximately 6617 plots, located on a sample grid spacing of 1.4 km. 900 of these plots belong to the Canton of Grisons and were considered in this study. Plots identified as non-forest through photointerpretation of aerial imagery were not visited in the field. Sample plots consist of two concentric circles: 200 m^2 for trees with diameters at breast height (DBH) between 12 and 36 cm, and 500 m^2 for trees with DBH $\geq$36 cm, respectively. This results in DBH measurements of approximately 11 trees per plot. To improve stem volume estimation, a sub-sample of the tariff trees is randomly selected (approximately two trees per plot), on which tree height and diameter at 7 m are also measured. Biomass is predicted for forest plots using allometric models at the single-tree level and then extrapolated to per-hectare values. The biomass of each tree is calculated as the sum of the biomass of its stem, large and small branches, foliage, and coarse roots, each of which is calculated separately based on the allometric relationship between biomass and the diameter at breast height. Tree biomass is then extrapolated to per-hectare biomass using tally tree extrapolation factors, which are defined based on whether the tree belongs to the 200 m^2 or 500 m^2 plot circle (Brändli and Hägeli, 2019).

D.5 Tuscany

The field reference data for Tuscany were obtained from the 2nd Italian NFI (INFC, 2003), which employs a three-phase, non-aligned systematic sampling design (Fattorini et al., 2006). Sampling units are randomly placed within 1 × 1 km grid cells to ensure spatial balance (Bocci et al., 2024). In the first phase, land use is classified via aerial photos. Then, a subsample is visited in the field to acquire qualitative data on forest type, management, and ownership. Finally, in the third phase, a subsample is subject to a quantitative field survey conducted in circular plots (13 m radius, 530 m^2) to collect biophysical measurements (INFC, 2003). The dataset used in this study is derived from the final phase and is freely available at https://www.inventarioforestale.org (Borghetti and Chirici, 2016; Pecchi et al., 2019). Trees GSV was estimated by using species-specific allometric models from the NFI, based on tree diameter and height (Tabacchi et al., 2011).

Data availability

Data will be made available on request.

References

Almeida, D.R.A. de, Broadbent, E.N., Ferreira, M.P., Meli, P., Zambrano, A.M.A., Gorgens, E.B., Resende, A.F., de Almeida, C.T., do Amaral, C.H., Corte, A.P.D., Silva, C.A., Romanelli, J.P., Prata, G.A., de Almeida Papa, D., Stark, S.C., Valbuena, R., Nelson, B.W., Guillemot, J., Féret, J.-B.B., Chazdon, R., Brancalion, P. H.S., 2021. Monitoring restored tropical forest diversity and structure through UAV-borne hyperspectral and lidar fusion. Remote Sens. Environ. 264, 112582. https://doi.org/10.1016/j.rse.2021.112582.

Alvites, C., O'Sullivan, H., Francini, S., Marchetti, M., Santopuoli, G., Chirici, G., Lasserre, B., Marignani, M., Bazzato, E., 2025. Canopy height Mapper: A google earth engine application for predicting global canopy heights combining GEDI with multi-source data. Environmental Modelling & Software 183, 106268. https://doi.org/10.1016/j.envsoft.2024.106268.

Andersen, H.-E., 2009. Using airborne light detection and ranging (LIDAR) to characterize forest stand condition on the kenai peninsula of Alaska. West. J. Appl. For. 24, 95–102. https://doi.org/10.1093/wjaf/24.2.95.

Arets, E.J.M.M., van der Kolk, J.W.H., Hengeveld, G.M., Lesschen, J.P., Kramer, H., Kuikman, P.J., Schellaas, M.J., 2019. Greenhouse Gas Reporting of the LULUCF Sector in the Netherlands 1–114.

Avitabile, V., Baccini, A., Friedl, M.A., Schmullius, C., 2012. Capabilities and limitations of landsat and land cover data for aboveground woody biomass estimation of Uganda. Remote Sens. Environ. 117, 366–380. https://doi.org/10.1016/j.rse.2011.10.012.

Ayzel, G., Heistermann, M., Winterrath, T., 2019. Optical flow models as an open benchmark for radar-based precipitation nowcasting (rainymotion v0.1). Geosci. Model Dev. (GMD) 12 (4), 1387–1402. https://doi.org/10.5194/gmd-12-1387-2019.

Bocci, C., Francini, S., Rocco, E., 2024. A new sampling strategy for enhancing forest monitoring leveraging remote sensing data. JABES. https://doi.org/10.1007/s13253-024-00670-6.

Bolton, D.K., Tompalski, P., Coops, N.C., White, J.C., Wulder, M.A., Hermosilla, T., Queinnec, M., Luther, J.E., van Lier, O.R., Fournier, R.A., Woods, M., Treitz, P.M., van Ewijk, K.Y., Graham, G., Quist, L., 2020. Optimizing landsat time series length for regional mapping of lidar-derived forest structure. Remote Sens. Environ. 239, 111645. https://doi.org/10.1016/j.rse.2020.111645.

Borghetti, M., Chirici, G., 2016. Raw Data from the Italian National Forest Inventory Are on-line and Publicly Available, 13. For. - Riv. di Selvic. ed Ecol. For., pp. 33–34. https://doi.org/10.3832/efor0083-013

Borghi, C., Francini, S., Pollastrini, M., Bussotti, F., Travaglini, D., Marchetti, M., Munafò, M., Scarascia-Mugnozza, G., Tonti, D., Ottaviano, M., 2021. MONITORING THIRTY-FIVE YEARS OF ITALIAN FOREST DISTURBANCE USING LANDSAT TIME SERIES. Planet Care from Sp, p. 112.

Brändli, U.-B., Hägeli, M., 2019. Swiss NFI at a glance, 3–35. https://doi.org/10.1007/978-3-030-19293-8_1.

Breidenbach, J., Nothdurft, A., Kändler, G., 2010. Comparison of nearest neighbour approaches for small area estimation of tree species-specific forest inventory attributes in central Europe using airborne laser scanner data. Eur. J. For. Res. 129, 833–846. https://doi.org/10.1007/s10342-010-0384-1.

Brouwer, F., Hellegers, P., 1996. The nitrate directive and farming practice in the european union. Eur. Environ. 6, 204–209.

Burrascano, S., Chianucci, F., Trentanovi, G., Kepfer-Rojas, S., Sitzia, T., Tinya, F., Doerfler, I., Paillet, Y., Nagel, T.A., Mitic, B., Morillas, L., Munzi, S., Van der Sluis, T., Alterio, E., Balducci, L., de Andrade, R.B., Bouget, C., Giordani, P., Lachat, T., Matosevic, D., Napoleone, F., Nascimbene, J., Paniccia, C., Roth, N., Aszalós, R., Brazaitis, G., Cutini, A., D'Andrea, E., De Smedt, P., Heilmann-Clausen, J., Janssen, P., Kozák, D., Mårell, A., Mikoláš, M., Nordén, B., Matula, R., Schall, P., Svoboda, M., Ujhazyova, M., Vandekerkhove, K., Wohlwend, M., Xystrakis, F., Aleffi, M., Ammer, C., Archaux, F., Asbeck, T., Avtzis, D., Ayasse, M., Bagella, S., Balestrieri, R., Barbati, A., Basile, M., Bergamini, A., Bertini, G., Biscaccianti, A.B., Boch, S., Bölöni, J., Bombi, P., Boscardin, Y., Brunialti, G., Bruun, H.H., Buscot, F., Byriel, D.B., Campagnaro, T., Campanaro, A., Chauvat, M., Ciach, M., Čiliak, M., Cistrone, L., Pereira, J.M.C., Daniel, R., De Cinti, B., De Filippo, G., Dekoninck, W., Di Salvatore, U., Dumas, Y., Elek, Z., Ferretti, F., Fotakis, D., Frank, T., Frey, J., Giancola, C., Gomoryová, E., Gosselin, M., Gosselin, F., Gossner, M.M., Götmark, F., Haeler, E., Hansen, A.K., Hertzog, L., Hofmeister, J., Hošek, J., Johannsen, V.K., Justensen, M.J., Korboulewsky, N., Kovács, B., Lakatos, F., Landivar, C.M., Lens, L., Lingua, E., Lombardi, F., Máliš, F., Marchino, L., Marozas, V., Matteucci, G., Mattioli, W., Møller, P.F., Müller, J., Németh, C., Ónodi, G., Parisi, F., Perot, T., Perret, S., Persiani, A.M., Portaccio, A., Posillico, M., Preikša, Ž., Rahbek, C., Rappa, N.J., Ravera, S., Romano, A., Samu, F., Scheidegger, C., Schmidt, I.K., Schwegmann, S., Sicuriello, F., Spinu, A.P., Spyroglou, G., Stillhard, J., Topalidou, E., Tøttrup, A.P., Ujházy, K., Veres, K., Verheyen, K., Weisser, W.W., Zapponi, L., Ódor, P., 2023. Where are we now with European forest multi-taxon biodiversity and where can we head to? Biol. Conserv. 284, 110176. https://doi.org/10.1016/j.biocon.2023.110176.

Cartus, O., Kellndorfer, J., Rombach, M., Walker, W., 2012. Mapping canopy height and growing stock volume using airborne lidar, ALOS PALSAR and landsat ETM+. Remote Sens. 4, 3320–3345. https://doi.org/10.3390/rs4113320.

Caruana, R., 1997. Multitask learning. Mach. Learn. 28 (1), 41–75. https://doi.org/10.1023/A:1007379606734.

Chirici, G., Giannetti, F., McRoberts, R.E., Travaglini, D., Pecchi, M., Maselli, F., Chiesi, M., Corona, P., 2020. Wall-to-wall spatial prediction of growing stock volume based on Italian national forest inventory plots and remotely sensed data. Int. J. Appl. Earth Obs. Geoinf. 84, 101959. https://doi.org/10.1016/j.jag.2019.101959.

Coops, N.C., Tompalski, P., Goodbody, T.R.H., Queinnec, M., Luther, J.E., Bolton, D.K., White, J.C., Wulder, M.A., van Lier, O.R., Hermosilla, T., 2021. Modelling lidar-derived estimates of forest attributes over space and time: a review of approaches and future trends. Rem. Sens. Environ. 260, 112477. https://doi.org/10.1016/j.rse.2021.112477.

Coppin, P.R., Bauer, M.E., 1996. Digital change detection in forest ecosystems with remote sensing imagery. Remote Sens. Rev. 13, 207–234. https://doi.org/10.1080/02757259609532305.

Crist, E.P., Cicone, R.C., 1984. Application of the tasseled cap concept to simulated thematic mapper data. Photogramm. Eng. Rem. Sens. 50, 343–352.

Davies, A.B., Asner, G.P., 2014. Advances in animal ecology from 3D-LiDAR ecosystem mapping. Trends Ecol. Evol. 29, 681–691. https://doi.org/10.1016/j.tree.2014.10.005.

de Lera Garrido, A., Gobakken, T., Hauglin, M., Næsset, E., Bollandsås, O.M., 2023. Accuracy assessment of the nationwide forest attribute map of Norway constructed

by using airborne laser scanning data and field data from the national forest inventory. Scand. J. For. Res. 38 (1–2), 9–22. https://doi.org/10.1080/02827581.2023.2184488.
Delgado-Fernández, M., Cernadas, E., Barro, S., Amorim, D., 2014. Do we need hundreds of classifiers to solve real world classification problems? J. Mach. Learn. Res. 15, 3133–3181.
Du, C., Fan, W., Ma, Y., Jin, H.-I., Zhen, Z., 2021. The effect of synergistic approaches of features and ensemble learning algorithms on aboveground biomass estimation of natural secondary forests based on ALS and landsat 8. Sensors 21 (17), 5974. https://doi.org/10.3390/s21175974.
D'Amico, Giovanni, Francini, S., Giannetti, F., Vangi, E., Travaglini, D., Chianucci, F., Mattioli, W., Grotti, M., Puletti, N., Corona, P., Chirici, G., 2021a. A deep learning approach for automatic mapping of poplar plantations using Sentinel-2 imagery. GIScience Remote Sens. 58, 1352–1368. https://doi.org/10.1080/15481603.2021.1988427.
D'Amico, Giovanni, Vangi, E., Francini, S., Giannetti, F., Nicolaci, A., Travaglini, D., Massai, L., Giambastiani, Y., Terranova, C., Chirici, G., 2021b. Are we ready for a national forest Information System? State of the art of forest maps and airborne laser scanning data availability in Italy. iForest - Biogeosciences For. 14, 144–154. https://doi.org/10.3832/ifor3648-014.
D'Amico, G., McRoberts, R.E., Giannetti, F., Vangi, E., Francini, S., Chirici, G., 2022. Effects of lidar coverage and field plot data numerosity on forest growing stock volume estimation. Eur. J. Remote Sens. 55, 199–212. https://doi.org/10.1080/22797254.2022.2042397.
D'Amico, G., Nilsson, M., Axelsson, A., Chirici, G., 2024. Data homogeneity impact in tree species classification based on Sentinel-2 multitemporal data case study in central Sweden. Int. J. Rem. Sens. 45, 5050–5075. https://doi.org/10.1080/01431161.2024.2371082.
EEA, 2016. Biogeographical regions [WWW Document]. URL. https://sdi.eea.europa.eu/data/c6d27566-e699-4d58-a132-bbe3fe01491b.
Ellison, D., Morris, C.E., Locatelli, B., Sheil, D., Cohen, J., Murdiyarso, D., Gutierrez, V., Noordwijk, M. van, Creed, I.F., Pokorny, J., Gaveau, D., Spracklen, D.V., Tobella, A. B., Ilstedt, U., Teuling, A.J., Gebrehiwot, S.G., Sands, D.C., Muys, B., Verbist, B., Springgay, E., Sugandi, Y., Sullivan, C.A., 2017. Trees, forests and water: cool insights for a hot world. Glob. Environ. Change 43, 51–61. https://doi.org/10.1016/j.gloenvcha.2017.01.002.
Erfanifard, Y., Lisiewicz, M., Stereńczak, K., 2024. High resolution remote sensing for biodiversity assessment and monitoring: a case study of dominant tree species in an old-growth forest. For. Ecol. Manage. 566, 122094. https://doi.org/10.1016/j.foreco.2024.122094.
Esteban, J., McRoberts, R., Fernández-Landa, A., Tomé, J., Næsset, E., 2019. Estimating forest volume and biomass and their changes using random forests and remotely sensed data. Remote Sens. 11, 1944. https://doi.org/10.3390/rs11161944.
European Commission, 1979. Council Directive 79/409/EEC of 2 April 1979 on the Conservation of Wild Birds.
European Commission, 1992. Council directive 92/43/ECC. Off. J. Eur. Union 94, 40–52.
European Commission, 2009. Common Implementation Strategy for the Water Framework Directive, 2000/60/Ec.
Fahey, T.J., Woodbury, P.B., Battles, J.J., Goodale, C.L., Hamburg, S.P., Ollinger, S.V., Woodall, C.W., 2010. Forest carbon storage: ecology, management, and policy. Front. Ecol. Environ. 8, 245–252. https://doi.org/10.1890/080169.
Fan, W., Tian, J., Knoke, T., Yang, B., Liang, F., Dong, Z., 2024. Investigating dual-source satellite image data and ALS data for estimating aboveground biomass. Remote Sens. 16 (10), 1804. https://doi.org/10.3390/rs16101804.
Fassnacht, F.E., White, J.C., Wulder, M.A., Næsset, E., 2024. Remote sensing in forestry: current challenges, considerations and directions. For. An Int. J. For. Res. 97, 11–37. https://doi.org/10.1093/forestry/cpad024.
FISE, 2021. Europe forest. https://forest.eea.europa.eu/countries/regions/european-union, 11.17.21.
Foga, S., Scaramuzza, P.L., Guo, S., Zhu, Z., Dilley, R.D., Beckmann, T., Schmidt, G.L., Dwyer, J.L., Hughes, M.J., Laue, B., 2017. Cloud detection algorithm comparison and validation for operational landsat data products. Rem. Sens. Environ. 194, 379–390. https://doi.org/10.1016/j.rse.2017.03.026.
Fogel, F., Perron, Y., Besic, N., Saint-André, L., Pellissier-Tanon, A., Schwartz, M., Boudras, T., Fayad, I., d'Aspremont, A., Landrieu, L., Ciais, P., 2024. Open-canopy: towards very high resolution forest monitoring. arXiv. https://doi.org/10.48550/arXiv.2407.09392.
Forest Data Bank, 2024. State forests national forest holding. https://www.bdl.lasy.gov.pl, 12.18.24.
Forzieri, G., Girardello, M., Ceccherini, G., Spinoni, J., Feyen, L., Hartmann, H., Beck, P. S.A., Camps-Valls, G., Chirici, G., Mauri, A., Cescatti, A., 2021. Emergent vulnerability to climate-driven disturbances in European forests. Nat. Commun. 12, 1081. https://doi.org/10.1038/s41467-021-21399-7.
Francini, S., McRoberts, R.E., D'Amico, G., Coops, N.C., Hermosilla, T., White, J.C., Wulder, M.A., Marchetti, M., Mugnozza, G.S., Chirici, G., 2022. An open science and open data approach for the statistically robust estimation of forest disturbance areas. Int. J. Appl. Earth Obs. Geoinf. 106, 102663. https://doi.org/10.1016/j.jag.2021.102663.
Francini, S., Cocozza, C., Hölttä, T., Lintunen, A., Paljakka, T., Chirici, G., Traversi, M.L., Giovannelli, A., 2023a. A temporal segmentation approach for dendrometers signal-to-noise discrimination. Comput. Electron. Agric. 210, 107925. https://doi.org/10.1016/j.compag.2023.107925.
Francini, S., Hermosilla, T., Coops, N.C., Wulder, M.A., White, J.C., Chirici, G., 2023b. An assessment approach for pixel-based image composites. ISPRS J. Photogramm. Remote Sens. 202, 1–12. https://doi.org/10.1016/j.isprsjprs.2023.06.002.
Francini, S., McRoberts, R.E., Giannetti, F., Mencucci, M., Marchetti, M., Scarascia Mugnozza, G., Chirici, G., 2020. Near-real time forest change detection using PlanetScope imagery. European Journal of Remote Sensing 53 (1), 233–244. https://doi.org/10.1080/22797254.2020.1806734.
Francini, S., Schelhaas, M.-J., Vangi, E., Lerink, B., Nabuurs, G.-J., McRoberts, R.E., Chirici, G., 2024. Forest species mapping and area proportion estimation combining Sentinel-2 harmonic predictors and national forest inventory data. Int. J. Appl. Earth Obs. Geoinf. 131, 103935. https://doi.org/10.1016/j.jag.2024.103935.
Fridman, J., Holm, S., Nilsson, M., Nilsson, P., Ringvall, A., Ståhl, G., 2014. Adapting national Forest inventories to changing requirements – the case of the Swedish national forest inventory at the turn of the 20th century. Silva Fenn. 48. https://doi.org/10.14214/sf.1095.
Gessler, A., Schaub, M., Bose, A., Trotsiuk, V., Valbuena, R., Chirici, G., Buchmann, N., 2024. Finding the balance between open access to forest data while safeguarding the integrity of national forest Inventory-derived information. New Phytol. 242, 344–346. https://doi.org/10.1111/nph.19466.
Ginzler, C., Hobi, M.L., 2015. Countrywide stereo-image matching for updating digital surface models in the framework of the Swiss national forest inventory. Remote Sens. 7, 4343–4370. https://doi.org/10.3390/rs70404343.
Gomes, V.C.F., Queiroz, G.R., Ferreira, K.R., 2020. An overview of platforms for big Earth observation data management and analysis. Remote Sens. 12, 1253. https://doi.org/10.3390/RS12081253.
Gong, Y., Zhu, D., Li, X., Lv, L., Zhang, B., Xuan, J., Du, H., 2024. Using UAV LiDAR intensity frequency and hyperspectral features to improve the accuracy of urban tree species classification. IEEE J. Sel. Top. Appl. Earth Obs. Rem. Sens. 17, 2849–2865. https://doi.org/10.1109/JSTARS.2023.3324475.
Gorelick, N., Hancher, M., Dixon, M., Ilyushchenko, S., Thau, D., Moore, R., 2017. Google Earth engine: planetary-Scale geospatial analysis for everyone. Remote Sens. Environ. 202, 18–27. https://doi.org/10.1016/j.rse.2017.06.031.
Gregoire, T.G., Næsset, E., McRoberts, R.E., Ståhl, G., Andersen, H.-E., Gobakken, T., Ene, L., Nelson, R., 2016. Statistical rigor in LiDAR-assisted estimation of aboveground forest biomass. Remote Sens. Environ. 173, 98–108. https://doi.org/10.1016/j.rse.2015.11.012.
Griffiths, P., van der Linden, S., Kuemmerle, T., Hostert, P., 2013. A pixel-based landsat compositing algorithm for large area land cover mapping. IEEE J. Sel. Top. Appl. Earth Obs. Rem. Sens. 6, 2088–2101. https://doi.org/10.1109/JSTARS.2012.2228167.
Hansen, M.C., Potapov, P.V., Moore, R., Hancher, M., Turubanova, S.A., Tyukavina, A., Thau, D., Stehman, S.V., Goetz, S.J., Loveland, T.R., Kommareddy, A., Egorov, A., Chini, L., Justice, C.O., Townshend, J.R.G., 2013. High-resolution global maps of 21st-century forest cover change. Science 342, 850–853. https://doi.org/10.1126/science.1244693.
Hawryło, P., Francini, S., Chirici, G., Giannetti, F., Parkitna, K., Krok, G., Mitelsztedt, K., Lisańczuk, M., Stereńczak, K., Ciesielski, M., Wężyk, P., Socha, J., 2020. The use of remotely sensed data and Polish NFI plots for prediction of growing stock volume using different predictive methods. Remote Sens. 12, 3331. https://doi.org/10.3390/rs12203331.
Healey, S.P., Yang, Z., Gorelick, N., Ilyushchenko, S., 2020. Highly local model calibration with a new GEDI LiDAR asset on google Earth engine reduces landsat forest height signal saturation. Remote Sens. 12, 2840.
Heaton, J., 2018. Ian Goodfellow, Yoshua Bengio, and Aaron Courville: Deep Learning. The mit press, pp. 305–307, 800 pp, isbn: 2016, 0262035618. Genet. Program. evolvable Mach. 19.
Hermosilla, T., Wulder, M.A., White, J.C., Coops, N.C., Hobart, G.W., 2015. An integrated landsat time series protocol for change detection and generation of annual gap-free surface reflectance composites. Remote Sens. Environ. 158, 220–234. https://doi.org/10.1016/j.rse.2014.11.005.
Hermoso, V., Carvalho, S.B., Giakoumi, S., Goldsborough, D., Katsanevakis, S., Leontiou, S., Markantonatou, V., Rumes, B., Vogiatzakis, I.N., Yates, K.L., 2022. The EU biodiversity strategy for 2030: opportunities and challenges on the path towards biodiversity recovery. Environ. Sci. Pol. 127, 263–271. https://doi.org/10.1016/j.envsci.2021.10.028.
Hettema, S., Rodgers, J., Sugiura, I., Twaddell, E., 2022. Boulder county disasters: mapping forest carbon stocks to understand carbon implications of treatment and wildfire (NASA technical report no. 20220005937). NASA Techn. Rep. Server. https://ntrs.nasa.gov/citations/20220005937Huete.
Hudak, A.T., Lefsky, M.A., Cohen, W.B., Berterretche, M., 2002. Integration of LiDAR and landsat ETM+ data for estimating and mapping forest canopy height. Rem. Sens. Environ. 82 (2–3), 397–416. https://doi.org/10.1016/S0034-4257(02)00056-1.
INFC, 2003. Manuale Di Fotointerpretazione per la Classificazione Delle Unità Di Campionamento Di Prima Fase 82.
Kennedy, R.E., Yang, Z., Cohen, W.B., 2010. Detecting trends in forest disturbance and recovery using yearly landsat time series: 1. LandTrendr — temporal segmentation algorithms. Remote Sens. Environ. 114, 2897–2910. https://doi.org/10.1016/j.rse.2010.07.008.
Keogh, E., Chu, S., Hart, D., Pazzani, M., 2001. An online algorithm for segmenting time series. In: Proceedings 2001 IEEE International Conference on Data Mining. IEEE Comput. Soc, pp. 289–296. https://doi.org/10.1109/ICDM.2001.989531.
Keogh, E., Chu, S., Hart, D., Pazzani, M., 2004. Segmenting time series: a survey and novel approach, 1–21. https://doi.org/10.1142/9789812565402_0001.
Key, C.H., Benson, N., 2006. Landscape assessment: ground measure of severity, the composite burn index; and remote sensing of severity. The Normalized Burn Ratio.
Lang, N., Jetz, W., Schindler, K., Wegner, J.D., 2022. A high-resolution canopy height model of the Earth. arXiv. http://arxiv.org/abs/2204.08322.
Lillesand, T., Kiefer, R.W., Chipman, J., 2015. Remote Sensing and Image Interpretation. John Wiley & Sons.

Liu, S., Brandt, M., Nord-Larsen, T., Chave, J., Reiner, F., Lang, N., Tong, X., Ciais, P., Igel, C., Pascual, A., Guerra-Hernandez, J., Li, S., Mugabowindekwe, M., Saatchi, S., Yue, Y., Chen, Z., Fensholt, R., 2023. The overlooked contribution of trees outside forests to tree cover and woody biomass across Europe. Sci. Adv. 9 (37), eadh4097. https://doi.org/10.1126/sciadv.adh4097.

Margolis, H.A., Nelson, R.F., Montesano, P.M., Beaudoin, A., Sun, G., Andersen, H.-E., Wulder, M.A., 2015. Combining satellite lidar, airborne lidar, and ground plots to estimate the amount and distribution of aboveground biomass in the boreal forest of North America. Can. J. For. Res. 45, 838–855. https://doi.org/10.1139/cjfr-2015-0006.

Mascaro, J., Asner, G.P., Muller-Landau, H.C., van Breugel, M., Hall, J., Dahlin, K., 2011. Controls over aboveground forest carbon density on Barro Colorado island. Panama. Biogeosciences 8, 1615–1629. https://doi.org/10.5194/bg-8-1615-2011.

Matasci, G., Hermosilla, T., Wulder, M.A., White, J.C., Coops, N.C., Hobart, G.W., Bolton, D.K., Tompalski, P., Bater, C.W., 2018a. Three decades of forest structural dynamics over Canada's forested ecosystems using landsat time-series and lidar plots. Remote Sens. Environ. 216, 697–714. https://doi.org/10.1016/j.rse.2018.07.024.

Matasci, G., Hermosilla, T., Wulder, M.A., White, J.C., Coops, N.C., Hobart, G.W., Zald, H.S.J., 2018b. Large-area mapping of Canadian boreal forest cover, height, biomass and other structural attributes using landsat composites and lidar plots. Remote Sens. Environ. 209, 90–106. https://doi.org/10.1016/j.rse.2017.12.020.

McRoberts, R.E., Tomppo, E.O., 2007. Remote sensing support for national forest inventories. Remote Sens. Environ. 110, 412–419. https://doi.org/10.1016/j.rse.2006.09.034.

McRoberts, R.E., Tomppo, E., Schadauer, K., Vidal, C., Ståhl, G., Chirici, G., Lanz, A., Cienciala, E., Winter, S., Smith, W.B., 2009. Harmonizing national forest inventories. J. For. 107, 179–187. https://doi.org/10.1093/jof/107.4.179.

McRoberts, R.E., Næsset, E., Saatchi, S., Quegan, S., 2022. Statistically rigorous, model-based inferences from maps. Remote Sens. Environ. 279, 113028. https://doi.org/10.1016/j.rse.2022.113028.

McRoberts, R.E., Næsset, E., Hou, Z., Ståhl, G., Saarela, S., Esteban, J., Travaglini, D., Mohammadi, J., Chirici, G., 2023. How many bootstrap replications are necessary for estimating remote sensing-assisted, model-based standard errors? Remote Sens. Environ. 288, 113455. https://doi.org/10.1016/j.rse.2023.113455.

Miettinen, J., Breidenbach, J., Adame, P., Adolt, R., Alberdi, I., Antropov, O., et al., 2025. Pan-european forest maps produced with a combination of earth observation data and national forest inventory plots. Data Brief 60, 111613. https://doi.org/10.1016/j.dib.2025.111613.

Müller, J., Brandl, R., 2009. Assessing biodiversity by remote sensing in mountainous terrain: the potential of LiDAR to predict forest beetle assemblages. J. Appl. Ecol. 46, 897–905. https://doi.org/10.1111/j.1365-2664.2009.01677.x.

Næsset, E., 1997a. Estimating timber volume of forest stands using airborne laser scanner data. Remote Sens. Environ. 61, 246–253. https://doi.org/10.1016/S0034-4257(97)00041-2.

Næsset, E., 1997b. Determination of mean tree height of forest stands using airborne laser scanner data. ISPRS J. Photogramm. Remote Sens. 52, 49–56. https://doi.org/10.1016/S0924-2716(97)83000-6.

Næsset, E., 2002. Predicting forest stand characteristics with airborne scanning laser using a practical two-stage procedure and field data. Remote Sens. Environ. 80, 88–99. https://doi.org/10.1016/S0034-4257(01)00290-5.

Næsset, E., Gobakken, T., 2008. Estimation of above- and below-ground biomass across regions of the boreal forest zone using airborne laser. Remote Sens. Environ. 112, 3079–3090. https://doi.org/10.1016/j.rse.2008.03.004.

Nelson, R., 2013. How did we get here? An early history of forestry lidar1. Can. J. Rem. Sens. 39, S6–S17. https://doi.org/10.5589/m13-011.

Nilsson, M., Nordkvist, K., Jonzén, J., Lindgren, N., Axensten, P., Wallerman, J., Egberth, M., Larsson, S., Nilsson, L., Eriksson, J., Olsson, H., 2017. A nationwide forest attribute map of Sweden predicted using airborne laser scanning data and field data from the national forest inventory. Remote Sens. Environ. 194, 447–454. https://doi.org/10.1016/j.rse.2016.10.022.

Nwankpa, C., Ijomah, W., Gachagan, A., Marshall, S., 2018. Activation functions: Comparison of trends in practice and research for deep learning. arXiv Prepr. arXiv1811.03378.

Omoniyi, T.O., Sims, A., 2024. Enhancing the precision of forest growing stock volume in the Estonian national forest inventory with different predictive techniques and remote sensing data. Remote Sens. 16 (20), 3794. https://doi.org/10.3390/rs16203794.

Ørka, H.O., Næsset, E., Bollandsås, O.M., 2009. Classifying species of individual trees by intensity and structure features derived from airborne laser scanner data. Remote Sens. Environ. 113, 1163–1174. https://doi.org/10.1016/j.rse.2009.02.002.

Ørka, H.O., Næsset, E., Bollandsås, O.M., 2010. Effects of different sensors and leaf-on and leaf-off canopy conditions on echo distributions and individual tree properties derived from airborne laser scanning. Remote Sens. Environ. 114, 1445–1461. https://doi.org/10.1016/j.rse.2010.01.024.

Orsi, F., Ciolli, M., Primmer, E., Varumo, L., Geneletti, D., 2020. Mapping hotspots and bundles of forest ecosystem services across the european union. Land Use Policy 99, 104840. https://doi.org/10.1016/J.LANDUSEPOL.2020.104840.

Palahí, M., Valbuena, R., Senf, C., Acil, N., Pugh, T.A.M., Sadler, J., Seidl, R., Potapov, P., Gardiner, B., Hetemäki, L., Chirici, G., Francini, S., Hlásny, T., Lerink, B.J.W., Olsson, H., González Olabarria, J.R., Ascoli, D., Asikainen, A., Bauhus, J., Berndes, G., Donis, J., Fridman, J., Hanewinkel, M., Jactel, H., Lindner, M., Marchetti, M., Marušák, R., Sheil, D., Tomé, M., Trasobares, A., Verkerk, P.J., Korhonen, M., Nabuurs, G.J., 2021. Concerns about reported harvests in European forests. Nature 592, E15–E17. https://doi.org/10.1038/s41586-021-03292-x.

Pecchi, M., Marchi, M., Giannetti, F., Bernetti, I., Bindi, M., Moriondo, M., Maselli, F., Fibbi, L., Corona, P., Travaglini, D., Chirici, G., 2019. Reviewing climatic traits for the main forest tree species in Italy. iForest - Biogeosciences For 12, 173–180. https://doi.org/10.3832/ifor2835-012.

Petersson, H., Ellison, D., Appiah Mensah, A., Berndes, G., Egnell, G., Lundblad, M., Lundmark, T., Lundström, A., Stendahl, J., Wikberg, P., 2022. On the role of forests and the forest sector for climate change mitigation in Sweden. GCB Bioenergy 14, 793–813. https://doi.org/10.1111/gcbb.12943.

Potapov, P., Li, X., Hernandez-Serna, A., Tyukavina, A., Hansen, M.C., Kommareddy, A., Pickens, A., Turubanova, S., Tang, H., Silva, C.E., Armston, J., Dubayah, R., Blair, J. B., Hofton, M., 2021. Mapping global forest canopy height through integration of GEDI and landsat data. Remote Sens. Environ. 253, 112165. https://doi.org/10.1016/j.rse.2020.112165.

Puliti, S., Saarela, S., Gobakken, T., Ståhl, G., Næsset, E., 2018. Combining UAV and Sentinel-2 auxiliary data for forest growing stock volume estimation through hierarchical model-based inference. Remote Sens. Environ. 204, 485–497. https://doi.org/10.1016/j.rse.2017.10.007.

Reichstein, M., Camps-Valls, G., Stevens, B., Jung, M., Denzler, J., Carvalhais, N., Prabhat, 2019. Deep learning and process understanding for data-driven Earth system science. Nature 566 (7743), 195–204. https://doi.org/10.1038/s41586-019-0912-1.

Saarela, S., Holm, S., Grafström, A., Schnell, S., Næsset, E., Gregoire, T.G., Nelson, R.F., Ståhl, G., 2016. Hierarchical model-based inference for forest inventory utilizing three sources of information. Ann. For. Sci. 73, 895–910. https://doi.org/10.1007/s13595-016-0590-1.

Saarela, S., Holm, S., Healey, S., Andersen, H.-E., Petersson, H., Prentius, W., Patterson, P., Næsset, E., Gregoire, T., Ståhl, G., 2018. Generalized hierarchical model-based estimation for aboveground biomass assessment using GEDI and landsat data. Remote Sens. 10, 1832. https://doi.org/10.3390/rs10111832.

Saarela, S., Healey, S.P., Yang, Z., Roald, B., Patterson, P.L., Gobakken, T., Næsset, E., Hou, Z., McRoberts, R.E., Ståhl, G., 2025. A separable bootstrap variance estimation algorithm for hierarchical model-based inference of forest aboveground biomass using data from <scp>NASA</scp> 's <scp>GEDI</scp> and landsat missions. Environmetrics 36. https://doi.org/10.1002/env.2883.

Saunders, J., Reeve, R., 2014. The EU Timber Regulation and CITES 30.

Schelhaas, M.J., Clerkx, A.P.P.M., Daamen, W.P., Oldenburger, J.F., Velema, G., Schnitger, P., Schoonderwoerd, H., Kramer, H., 2014. Zesde Nederlandse bosinventarisatie; methoden en basisresultaten. Wageningen Alterra-rapport 2545, 98.

Schmidt, G., Jenkerson, C.B., Masek, J., Vermote, E., Gao, F., 2013. Landsat ecosystem disturbance adaptive processing system (LEDAPS) algorithm description. Open File Rep. https://doi.org/10.3133/ofr20131057.

Schöpe, M., 2008. Renewable energy directive. Eur. Wind Energy Conf. Exhib. 1, 32–38, 2008.

Schwartz, M., Ciais, P., De Truchis, A., Chave, J., Ottlé, C., Vega, C., et al., 2023. FORMS: forest multiple source height, wood volume, and biomass maps in France at 10 to 30 m resolution based on Sentinel-1, Sentinel-2, and GEDI data with a deep learning approach. Earth Syst. Sci. Data 15 (11), 4927–4945. https://doi.org/10.5194/essd-15-4927-2023.

Seely, H., Coops, N.C., White, J.C., Montwé, D., 2025. Forest aboveground biomass estimation using deep learning data fusion of ALS, multispectral, and topographic data. Int. J. Rem. Sens. 46 (9), 3874–3893. https://doi.org/10.1080/01431161.2025.2492412.

Shi, Y., Wang, T., Skidmore, A.K., Heurich, M., 2018. Important LiDAR metrics for discriminating forest tree species in central Europe. ISPRS J. Photogramm. Remote Sens. 137, 163–174. https://doi.org/10.1016/j.isprsjprs.2018.02.002.

Skinner, I., 2006. The thematic strategy on air pollution - under the microscope. Concawe Rev. 15.

Srivastava, N., Hinton, G., Krizhevsky, A., Sutskever, I., Salakhutdinov, R., 2014. Dropout: a simple way to prevent neural networks from overfitting. J. Mach. Learn. Res. 15, 1929–1958.

Staben, G.W., Lucieer, A., Scarth, P., 2018. Modelling LiDAR-derived tree canopy height from landsat TM, ETM+ and OLI satellite imagery – a machine learning approach. Int. J. Appl. Earth Obs. Geoinf. 73, 666–681. https://doi.org/10.1016/j.jag.2018.08.01.

Ståhl, G., Heikkinen, J., Ginzler, C., Winter, S., McRoberts, R.E., Hafrén, J., 2016. The role of national forest inventories in assessing adaptive capacity to climate change. For. Ecol. Manage.

Su, Y., Guo, Q., Xue, B., Hu, T., Alvarez, O., Tao, S., Fang, J., 2016. Spatial distribution of forest aboveground biomass in China: estimation through combination of spaceborne lidar, optical imagery, and forest inventory data. Remote Sens. Environ. 173, 187–199. https://doi.org/10.1016/j.rse.2015.12.002.

Tabacchi, G., Di Cosmo, L., Gasparini, P., 2011. Aboveground tree volume and phytomass prediction equations for forest species in Italy. Eur. J. For. Res. 130, 911–934.

Tolan, J., Yang, H.-I., Nosarzewski, B., Couairon, G., Vo, H.V., Brandt, J., et al., 2024. Very high resolution canopy height maps from RGB imagery using self-supervised vision transformer and convolutional decoder trained on aerial lidar. Rem. Sens. Environ. 300, 113888. https://doi.org/10.1016/j.rse.2023.113888.

Van Stan, J.T., Norman, Z., Meghoo, A., Friesen, J., Hildebrandt, A., Côté, J.-F., Underwood, S.J., Maldonado, G., 2017. Edge-to-Stem variability in wet-canopy evaporation from an urban tree row. Boundary-Layer Meteorol. 165, 295–310. https://doi.org/10.1007/s10546-017-0277-7.

Vauhkonen, J., 2018. Predicting the provisioning potential of forest ecosystem services using airborne laser scanning data and forest resource maps. For. Ecosyst. 5. https://doi.org/10.1186/s40663-018-0143-1.

Villikka, M., Packalén, P., Maltamo, M., 2012. The suitability of leaf-off airborne laser scanning data in an area-based forest inventory of coniferous and deciduous trees. Silva Fenn. 46. https://doi.org/10.14214/sf.68.

White, J.C., Wulder, M.A., Hobart, G.W., Luther, J.E., Hermosilla, T., Griffiths, P., Coops, N.C., Hall, R.J., Hostert, P., Dyk, A., Guindon, L., 2014. Pixel-based image compositing for large-area dense time series applications and science. Can. J. Rem. Sens. 40, 192–212. https://doi.org/10.1080/07038992.2014.945827.

White, J.C., Coops, N.C., Wulder, M.A., Vastaranta, M., Hilker, T., Tompalski, P., 2016. Remote sensing technologies for enhancing forest inventories: a review. Can. J. Rem. Sens. 42, 619–641. https://doi.org/10.1080/07038992.2016.1207484.

Withana, S., Baldock, D., Farmer, A., Pallemaerts, M., Hjerp, P., Watkins, E., Armstrong, J., Medarova-Bergstrom, K., Gantioler, S., 2010. Strategic Orientations of EU Environmental Policy Under the Sixth Environment Action Programme and Implications for the Future 136.

Wulder, M.A., Coops, N.C., 2014. Make Earth observations open access. Nature 513 (7516), 30–31. https://doi.org/10.1038/513030.

Wulder, M.A., Masek, J.G., Cohen, W.B., Loveland, T.R., Woodcock, C.E., 2012. Opening the archive: how free data has enabled the science and monitoring promise of landsat. Remote Sens. Environ. 122, 2–10. https://doi.org/10.1016/j.rse.2012.01.010.

Wulder, M.A., Roy, D.P., Radeloff, V.C., Loveland, T.R., Anderson, M.C., Johnson, D.M., Healey, S., Zhu, Z., Scambos, T.A., Pahlevan, N., Hansen, M., Gorelick, N., Crawford, C.J., Masek, J.G., Hermosilla, T., White, J.C., Belward, A.S., Schaaf, C., Woodcock, C.E., Huntington, J.L., Lymburner, L., Hostert, P., Gao, F., Lyapustin, A., Pekel, J.-F., Strobl, P., Cook, B.D., 2022. Fifty years of landsat science and impacts. Remote Sens. Environ. 280, 113195. https://doi.org/10.1016/j.rse.2022.113195.

Zald, H.S.J., Wulder, M.A., White, J.C., Hilker, T., Hermosilla, T., Hobart, G.W., Coops, N.C., 2016. Integrating landsat pixel composites and change metrics with lidar plots to predictively map forest structure and aboveground biomass in Saskatchewan, Canada. Remote Sens. Environ. 176, 188–201. https://doi.org/10.1016/j.rse.2016.01.015.

Zhang, L., Shao, Z., Liu, J., Cheng, Q., 2019. Deep learning-based retrieval of forest aboveground biomass from combined LiDAR and landsat 8 data. Remote Sens. 11 (12), 1459. https://doi.org/10.3390/rs11121459.

Zhou, Z.-H., Wu, J., Tang, W., 2002. Ensembling neural networks: many could be better than all. Artif. Intell. 137 (1–2), 239–263. https://doi.org/10.1016/S0004-3702(02)00190-X.